



**FUNDAMENTALS OF FLUID FILM JOURNAL BEARING OPERATION AND MODELING**

**Minhui He**

Machinery Specialist  
 BRG Machinery Consulting, LLC  
 Charlottesville, Virginia, USA

**C. Hunter Cloud**

President  
 BRG Machinery Consulting, LLC  
 Charlottesville, Virginia, USA

**James M. Byrne**

Machinery Specialist  
 BRG Machinery Consulting, LLC  
 Charlottesville, Virginia, USA

**José A. Vázquez**

Machinery Consultant  
 BRG Machinery Consulting, LLC  
 Wilmington, Delaware, USA



*Minhui He is a Machinery Specialist with BRG Machinery Consulting LLC, in Charlottesville, Virginia. His responsibilities include vibration troubleshooting, rotordynamic analysis, as well as bearing and seal analysis and design. He is also conducting research on rotordynamics and hydrodynamic bearings.*

*Dr. He received his B.S. degree (Chemical Machinery Engineering, 1994)*

*from Sichuan University. From 1996 to 2003, he conducted research on fluid film journal bearings in the ROMAC Laboratories at the University of Virginia, receiving his Ph.D. (Mechanical and Aerospace Engineering, 2003). He is a member of ASME, STLE, and the advisory committee for the Texas A&M Asia Turbomachinery and Pump Symposium.*



*C. Hunter Cloud is President of BRG Machinery Consulting, LLC, in Charlottesville, Virginia. He began his career with Mobil Research and Development Corporation in Princeton, NJ, as a turbomachinery specialist responsible for application engineering, commissioning, and troubleshooting for production, refining and chemical facilities. During his 11 years at Mobil, he*

*worked on numerous projects, including several offshore gas injection platforms in Nigeria as well as serving as reliability manager at a large US refinery.*

*Dr. Cloud received his B.S. (Mechanical Engineering, 1991) and Ph.D. (Mechanical and Aerospace Engineering, 2007) from the University of Virginia. He is a member of ASME, the Vibration Institute, the API 684 rotordynamics task force, and the advisory committee for the Texas A&M Turbomachinery Symposium.*



*James M. Byrne is a member of the BRG Machinery Consulting team in Charlottesville, Virginia. BRG provides a wide variety of machinery consulting services including design and analysis, selection, auditing, commissioning and troubleshooting. Mr. Byrne began his career designing internally geared centrifugal compressors for Carrier in Syracuse, New*

*York. He continued his career at Pratt and Whitney aircraft engines and became a technical leader for rotordynamics. Later, Mr. Byrne became a program manager for Pratt and Whitney Power Systems managing the development of new gas turbine products. From 2001 to 2007, he was President of Rotating Machinery Technology, a manufacturer of tilting pad bearings.*

*Mr. Byrne holds a BSME degree from Syracuse University, an MSME degree from the University of Virginia, and an MBA from Carnegie Mellon University. He is a member of the API 613 special purpose gear unit task force.*



*José Vázquez is a Machinery Consultant at BRG Machinery Consulting, LLC. He has over 25 years of experience in machinery analysis and troubleshooting. Prior to joining BRG, he worked for 10 years at DuPont as a Mechanical Consultant, primarily solving machinery problems and developing advanced measurement techniques.*

*Dr. Vázquez received his B.S. (Mechanical Engineering, 1990) and MS (Specialization in Rotating Equipment, 1993) from the Universidad Simón Bolívar in Venezuela. He received his Ph.D. (Mechanical and Aerospace Eng., 1999) from the University of Virginia. He is a member of ASME.*

**ABSTRACT**

Widely used in turbomachinery, the fluid film journal bearing is critical to a machine’s overall reliability level. Their design complexity and application severity continue to increase making it challenging for the plant machinery engineer to



evaluate their reliability. This tutorial provides practical knowledge on their basic operation and what physical effects should be included in modeling a bearing to help ensure its reliable operation in the field. All the important theoretical aspects of journal bearing modeling, such as film pressure, film and pad temperatures, thermal and mechanical deformations and turbulent flow are reviewed.

Through some examples, the tutorial explores how different effects influence key performance characteristics like minimum film thickness, Babbitt temperature as well as stiffness and damping coefficients. Due to their increasing popularity, the operation and analysis of advanced designs using directed lubrication principles, such as inlet grooves and associated starvation issues, are also examined with several examples including comparisons to manufacturers' test data.

## INTRODUCTION

The objectives of this tutorial are to provide each student the following with respect to fluid film journal bearings:

- A basic understanding of their physics and operational considerations
- A basic understanding of their modeling fundamentals
- The knowledge to better interpret more advanced papers and topics
- A good reference source for the future

This tutorial is not:

- A design guideline. We do not intend to teach you how to design a bearing for any particular application. The literature is replete with fine design guidelines including those by Nicholas and Wygant (1995).
- A bearing primer. We expect the student to have a basic understanding of fluid film bearings, their use and basic operation. We do not describe all types of bearings, nor the evolution of their design.
- A thrust bearing tutorial. We focus solely on journal bearings, although many of the topics and much of the physics is also applicable to thrust bearings.

The authors' primary audience is plant machinery engineer evaluating new versus old designs to fix their machinery problems as well as central engineering machinery specialists in charge of selecting and auditing bearing designs for new machinery. Our goal is to prepare these individuals to ask good questions of those performing a bearing design or analysis. Plant engineers must understand the limits of any analysis so that they can manage risk and assess alternatives.

Bearing designers will also find the material useful in supplementing their expertise. These individuals must understand the underlying physics behind the computer program they are running. They too must understand the limitations and risks associated with their analysis. They must understand all of the options and inputs to their bearing code, plus understand what the output is telling them.

Why are the fundamentals of journal bearing operation and modeling important?

- Designs are more and more aggressive with less margin for error.
- Loads and speeds continue to increase in new machinery.
- While the basic fluid dynamics of fluid film bearings are well understood, secondary effects such as elastic deformations, heat transfer to the solids and turbulence are less well established.
- Innovation breeds new designs and technologies that cause the old analysis methods to fall short.
- The desire for lower power loss and lower oil consumption.
- The desire for improved reliability forces better understanding.
- The cost of redesign (trial and error) is enormous.
- The cost of a plant outage is greater.
- You can't test everything!

How does a poor bearing design manifest itself?

- High bearing metal temperatures, eventually leading to bearing failure
- High machinery vibrations
- Excessive power loss
- Excessive oil consumption

What are some common operational limits?

- Surface speeds: in the old days, less than 61 m/s (200 ft/s); today, up to 137 m/s (450 ft/s).
- Unit or specific load,  $W_U$ : in the old days, less than 17 bar (250 psi); today, up to 62 bar (900 psi).
- Babbitt lined bearings typically operate below 93 °C (200°F), while alternative materials and lubricants can run above 121°C (250°F).
- Film thickness values must typically be greater than 25  $\mu\text{m}$  (0.001 in). Discussions on minimum film thickness can be found in Martin and Garner (1973).

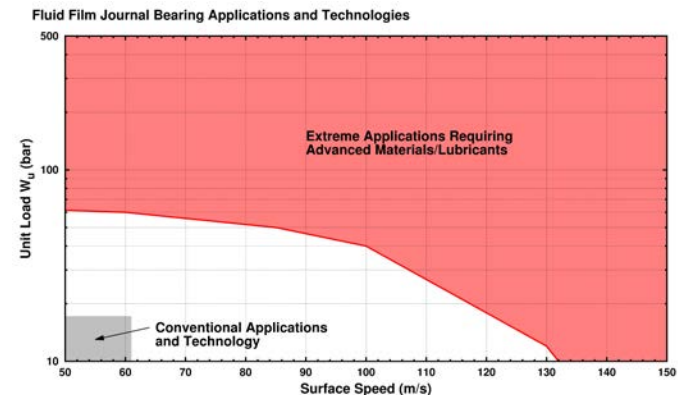


Figure 1. Journal Bearing Operational Limits

As shown in Figure 1, the operational limits have been greatly extended using new technologies. Thirty years ago, the designs outside of the gray box would have been ruled out as too aggressive. Today, many of them in the white region perform reliably as a result of advanced design features and the tools

necessary to model and predict their performance. Operation can even be extended into the red region of extreme applications.

Figure 2 shows the oil film shape, temperature distribution (the color contours) and pressure profile of one extreme application. In this case, the unit load is above 138 bar (2000 psi); the maximum temperature reaches 177°C (350°F); and the minimum film thickness is well below 10 μm (0.0004 in). Even under these extreme operating conditions, modern technologies, including special material coating, allow this bearing to operate successfully.

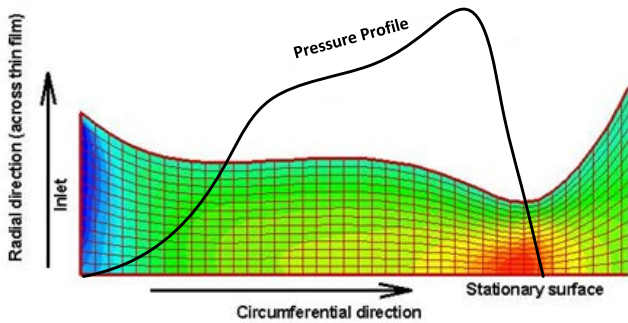


Figure 2. Example of an Extreme Application

The first section of this tutorial begins with a discussion of the operational aspects of fluid film bearings. Bearing geometrical aspects are discussed and the basic physics of fluid film bearing operation are developed. The second section uses what we learned in the operational section and describes the means by which we can model or predict fluid film bearing behavior.

## OPERATION

The operational characteristics of a journal bearing can be categorized into steady state and dynamic aspects. Steady state characteristics include a bearing's load capacity, pad temperature, power loss and the amount of oil required during operation. A bearing's load capacity is often measured using either eccentricity ratio that relates directly to its minimum film thickness, or the maximum pad temperature. A bearing's dynamic performance is typically characterized by its stiffness and damping properties. How these properties interact with the rotor system determines a machine's overall vibrational behavior.

The main objective of this section is to provide a general understanding of the basic physics that governs a bearing's steady state and dynamic operation. By comparing several common bearing designs, the key performance issues of interest will be examined. At the end of this section, one should understand the following:

- Development of hydrodynamic pressure or load capacity
- Relationships between viscous shearing, temperature rise, power loss and load capacity
- General influence of dynamic coefficients on rotordynamics including stability

- Speed and load dependency of steady state and dynamic properties
- Different behaviors of fixed geometry and tilting pad bearings

### Geometrical Parameters

Before discussing the operational aspects of journal bearings, some basic geometric parameters need to be defined. Figure 3(a) shows an arbitrary bearing pad of axial length  $L$  and arc length  $\theta_p$ . The pad supports the journal of radius  $R_j$  rotating at speed  $\omega$ . The radial clearance,  $c = R_b - R_j$ , allows the journal to operate at some eccentric position defined by distance  $e$  and attitude angle  $\Phi$ . The attitude angle is measured with respect to the direction of the applied load  $W$  and the line of centers. For a fixed geometry bearing, the line of centers establishes the minimum film thickness location. However, this is generally not true for a tilting pad bearing. Instead, the trailing edge of a tilting pad often becomes the minimum film thickness point.

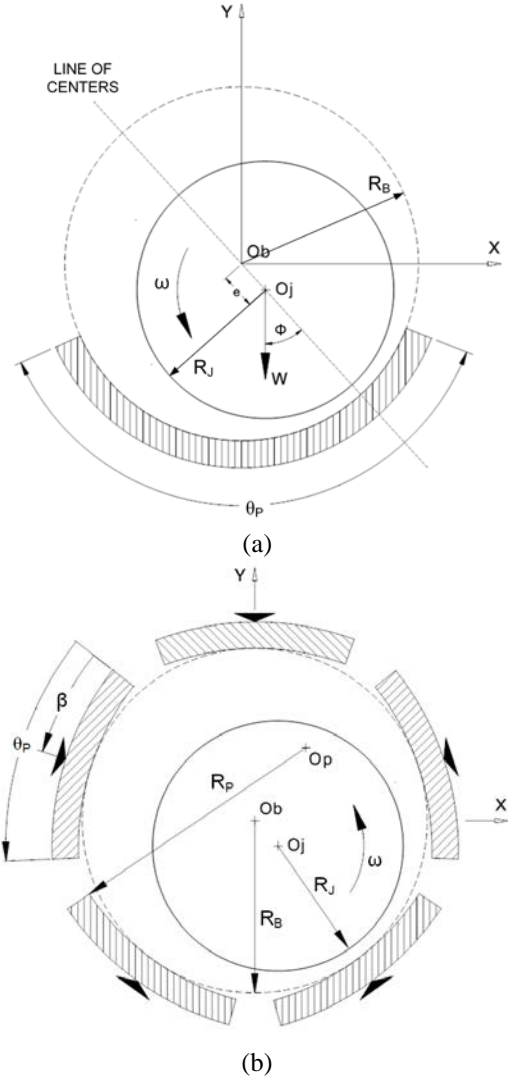


Figure 3. Bearing Geometry



Since typically the journal position relative to the bearing is of interest, an eccentricity ratio is defined using the radial clearance:

$$E = \frac{e}{c} = \sqrt{E_x^2 + E_y^2} \quad (1)$$

$$E_x = \frac{e_x}{c}, \quad E_y = \frac{e_y}{c}$$

At rest, normally the eccentricity ratio E would be expected to be 1.0 with the journal sitting on the bearing pad. E can be greater than 1.0 if the shaft sits between two tilting pads.

Figure 3(b) defines some other key geometric parameters with respect to a tilting pad bearing. The pad pivot offset is given by the ratio

$$\alpha = \frac{\beta}{\theta_p} \quad \text{Pivot Offset} \quad (2)$$

Centrally pivoted pads (50% offset or  $\alpha = 0.5$ ) are the commonly applied. However, 55 to 60 percent pivot offsets are often seen in high speed/load applications because of their relatively low pad temperatures (Simmons and Lawrence, 1996).

While the bearing assembly radius  $R_b$  determines the largest possible shaft size that can fit in the bearing, the individual pads may be machined to a different radius indicated by  $R_p$ . These radii along with  $R_j$  establish a very important bearing design parameter, preload or preset, which is defined by two clearances:

$$c_b = R_b - R_j \quad \text{Assembled or Set Bore Clearance} \quad (3)$$

$$c_p = R_p - R_j \quad \text{Pad Machined Clearance}$$

Preload or preset, m, is subsequently defined using their ratio

$$m = 1 - \left( \frac{c_b}{c_p} \right) \quad (4)$$

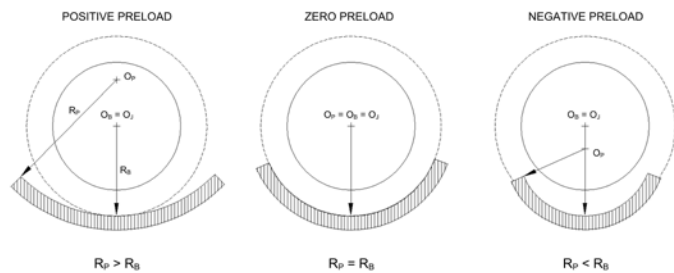


Figure 4. Pad Preload

Figure 4 shows how preload affects the relative film shapes within the bearing. For  $m = 0.0$ , the pad radius and assembly radius are equal. Typically, preload values are positive which, as shown in Figure 4, causes the shaft/bearing center ( $O_j = O_b$ ) to sit lower relative to the pad center  $O_p$ . Thus, one develops the connotations of *preloading* the bearing. While many associate

preload with only tilting pad bearings, it can also be used in the design of fixed geometry bearings. A lemon bore or elliptical bearing is the most common example (Salamone, 1984).

All of these geometric design parameters can significantly affect a bearing's steady state and dynamic characteristics. For example, tighter clearance and higher preload usually leads to greater load capacity and higher stiffness. Smaller clearance usually means higher Babbitt temperature, etc. In this tutorial, however, we will predominately focus on the influences of the operating parameters, such as shaft speed and bearing load. Excellent discussions on the effects of various geometric parameters can be found in Jones and Martin (1979) and Nicholas (1994).

### Steady State Performance

To be classified as a bearing, a device must fundamentally carry a load between two components. A journal bearing must accomplish this task while the shaft rotates and with minimum wear or failure. Inadequate load capacity leads to either rubbing contact between the journal and bearing surfaces, or thermal failure of the lubricant or bearing materials. Therefore, our first step is to explain the load carrying mechanism in a fluid film bearing.

### Local Capacity

Section summary:

- A convergent wedge, surface motion and viscous lubricant are necessary conditions to generate hydrodynamic pressure or load capacity in steady state operation.
- Typical pressure profiles, journal eccentricity ratios and centerline loci are shown through examples of three common designs.
- Hydrodynamic forces in fixed geometry bearings have strong cross-coupled components. Such cross coupling is usually negligible in tilting pad bearings due to the pads' ability to rotate.

In the early 1880's, the underlying physics of how a fluid film journal bearing supports a loaded and rotating shaft was a mystery. Using some of the lessons learned from pioneers in this field, the authors will examine the most important physical phenomena governing a bearing's load capacity: hydrodynamic pressure.

The concept of hydrodynamic lubrication was born from the experimental work of Beauchamp Tower (1883, 1885). Commissioned to study the frictional losses in railroad bearings (Pinkus, 1987), Tower encountered a persistent oil leak when he decided to drill an oiler hole in his bearing (Figure 5). After a cork and wooden plug were blown out of the hole, Tower realized that the lubricating oil was becoming pressurized. Tower altered his design such that the oil was supplied through two axial grooves which allowed him to install pressure gauges on the bearing surface. Figure 6 shows an example of the resultant pressures that Tower measured. Integrating this pressure distribution, Tower discovered that it equaled the load

he applied on the bearing. In one experiment, Tower's pressure profile integration yielded a film force of 7988 lbf (35.5 kN) compared with the applied load of 8008 lbf (35.6 kN), an amazingly accurate result (Dowson, 1998).

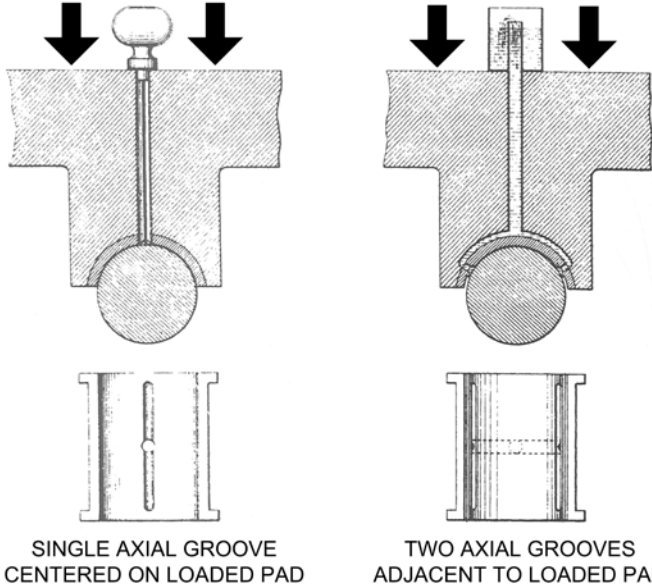


Figure 5. Tower's Experimental Bearings (Courtesy Tower, 1883)

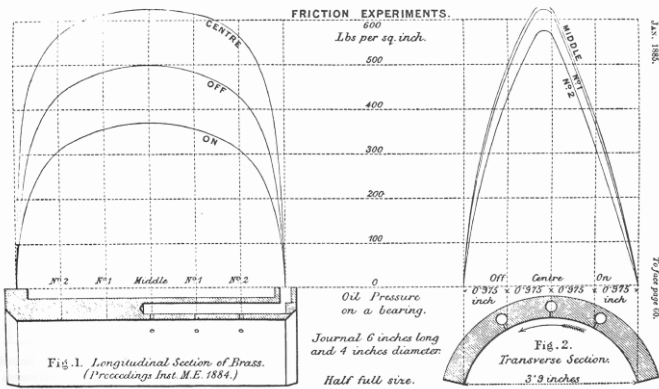


Figure 6. Tower's Pressure Measurements (Courtesy Tower, 1883)

While Tower was conducting his experiments, Osborne Reynolds (1886) derived the theoretical justification for the load carrying capacity of such journal bearings. He found that a fluid's pressure would increase when it is dragged by a moving surface into a decreasing clearance, like the plane slider situation shown in Figure 7(a). Such a situation demonstrates the governing principle of hydrodynamic lubrication. *Without relative motion or a converging clearance, no pressure or load capacity will be developed.* It is the pressure in the lubricant film that carries the external load and separates the solid surfaces, which further confirmed Tower's observations.

Figure 7(b) and (c) show two other examples of fluid being

dragged into a convergent clearance. The journal creates such convergent clearance because of its eccentric operation and/or the radii difference between it and the pad. For a perfectly centered journal with a zero preloaded pad, the inlet film thickness equals the minimum or outlet film thickness ( $h_i = h_o$ ) and we would expect no pressure to be developed in the film. The phenomenon of hydroplaning is another good example. Here the tire deformation creates a converging clearance that generates enough pressure in the water film to support the weight of the car. Both situations can be treated like the plane slider with  $h_i > h_o$ .

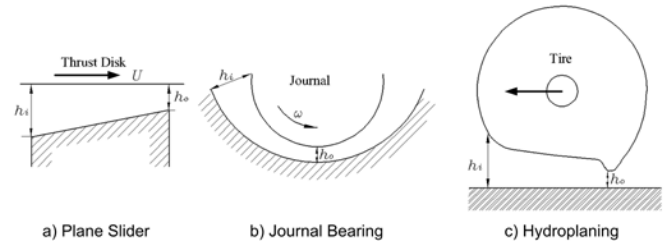


Figure 7. Examples of Hydrodynamic Lubricant

This section is focused on steady state operation in which the shaft has pure rotation and the wedge shape remains invariant in time. However, if the shaft is translating, the resulting squeeze motion can generate hydrodynamic pressure as well. Such situation is demonstrated by a squeeze film damper, which is basically a bearing with only translational motion. The pure squeeze motion produces hydrodynamic pressure, providing damping force to the system.

To understand the pressures distributions and the film forces developed in some typical journal bearing designs, here we examine a two axial groove bearing (often referred to as a plain journal bearing (Salamone, 1984)), a pressure dam bearing and a tilting pad bearing with four pads (Figure 8(a)). With the same diameter, axial length, bore clearance, preload, oil viscosity and speed, Figure 8(b) displays each bearing's circumferential pressure distribution. Each bearing has its journal position fixed downward halfway within the clearance at  $E_x = 0.0$  and  $E_y = -0.5$  (shown by the small blue square in the polar plot).

The two axial groove's pressure distribution in Figure 8 (b) has a peak pressure over 750 psig (52 bar). It is important to notice that the pressure distribution is not symmetric about this peak. Furthermore, the peak pressure does not occur at the minimum film thickness position ( $270^\circ$ ) where one would instinctively anticipate. These two pressure distribution characteristics are fundamental to all bearing types where hydrodynamic pressures are developed

No pressure is developed in the upper half of the bearing because of the diverging clearance and the relatively low oil supply pressure (20 psig or 1.4 bar). This condition, which exists in most fixed geometry bearings, causes the film to cavitate and restricts the pressure in the film to the ambient pressure. Physically on a cavitated pad, the fluid film is ruptured and the rotating shaft drags streamlets across this region (Heshmat, 1991). The film's positive pressure area results in a 6111 N

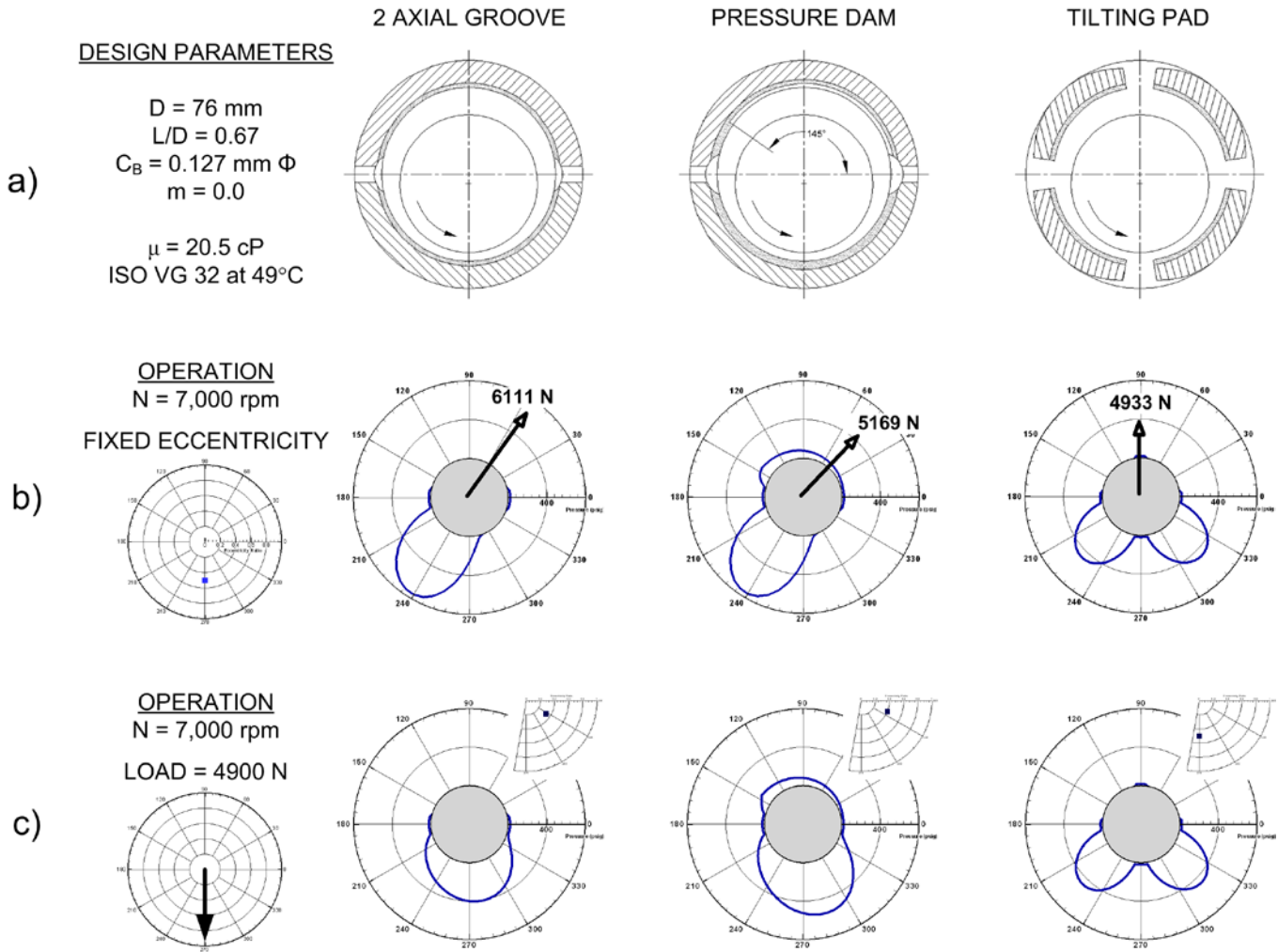


Figure 8. Pressure Profiles for Three Bearing Designs

effective force on the shaft at an angle of 56 degree.

Recalling that the journal was displaced vertically downward only, one should notice that the fluid film has now generated a responding force with a significant *horizontal* component. Such a reaction is the main reason plain journal bearings create such dynamic stability concerns. A cross coupling is experienced since movement in one direction causes a force component in the perpendicular direction. This behavior will be discussed further with respect to dynamic characteristics.

Since its lower half film profile is the same as that of the two axial groove bearing, the pressure dam bearing has an identical pressure distribution in its lower half. However, because of the presence of the dam, the upper half now has a converging wedge which generates a positive pressure profile. The peak pressure occurs at the dam location. With the upper half pressure counteracting the pressure developed in the lower half, the force exerted on the shaft has slightly reduced in magnitude to 5169 N and rotated more horizontally in direction.

Film pressure is developed on the bottom two pads of the

tilting pad bearing. At steady state, the moments on a pad must be balanced in order for the pad to reach an equilibrium tilt angle. When this occurs, the pad pressure force vector passes directly through the pivot. Unlike the two axial groove and pressure dam bearings, the tilting pad has produced a resultant film force that is almost purely vertical. In this case, a vertical displacement of the journal has resulted in an almost directly vertical force. This desirable characteristic totally relies on the pad's ability to tilt even though the tilt angles are very small (on the order of 0.01 degree). Boyd and Raimondi (1953) were among the first to explain this behavior while at Westinghouse. Both they and Hagg (1946) realized the implications from the dynamics standpoint, which will be discussed later

As a final point on Figure 8(b), one should notice the additional reduction in the tilting pad bearing's film force magnitude (4933 N versus 6111 N for the two axial groove bearing). This is expected since the pad area that carries load has been reduced. The two axial groove bearing has 150° of lower half pad arc length, while the tilting pad bearing has only  $2 \times 72^\circ = 144^\circ$  with a supply groove in between.

While good for demonstrating film forces and their non-linear nature, setting the journal at a fixed eccentricity like in Figure 8(b) does not represent a realistic operating condition. In reality, the bearing will adjust the shaft's position till the hydrodynamic force balances the applied load  $W$ . For the same three bearings, Figure 8(c) shows the pressure profiles when a constant load ( $W=4900$  N) is applied downward at  $270^\circ$ . Also shown are the resultant shaft eccentricity ratios where the shaft has reached its steady state equilibrium position (shown by the small blue square in the polar plot).

Comparing Figures 8(b) and (c), the journal inside the two axial groove bearing has now had to shift horizontally in order to create a film profile that only opposes the vertical load. This is evident in the more vertical orientation of the pressure distribution. Similar behavior is observed for the pressure dam bearing. However, because of the pressures created by the dam and its angular orientation, the shaft reaches a position of higher eccentricity and greater attitude angle than the two axial groove bearing. Both fixed geometry bearings are able to support the load at a lower eccentricity than the tilting pad bearing. This higher load capacity is expected when one recalls the resultant film forces created in Figure 8(b).

One should now have a basic feel for the pressures developed by hydrodynamic lubrication. Through different bearing geometries, we've seen how different converging wedges create different pressure distributions, and thus, various abilities to support load. What has not been emphasized is the importance of the lubricant's viscosity which determines the pressure generation just as much as the bearing's geometry.

As the next section will describe in detail, the lubricant's viscosity will decrease because of the internal heat generated during operation. Our discussions and comparisons, so far, have kept the viscosity constant or isoviscous. With this restriction removed, Figure 9 demonstrates that a bearing's load capacity is a strong function of its operating condition. In Figure 9(a), the load is fixed at 4900 N and the shaft speed varies from 1000 rpm to 19000 rpm. When stationary, the shaft sits on the bottom with zero attitude angle and unity eccentricity ratio (for the tilt pad bearing, the eccentricity is slightly higher because the shaft rests between the pads). As the shaft accelerates, the journal is lifted higher and higher by increasing hydrodynamic pressure.

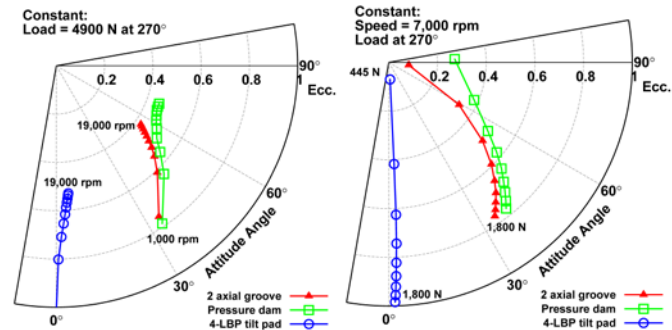


Figure 9. Load Capacity Trends Allowing for Viscosity Degradation Effects (Theoretical Predictions)

Although all three bearings exhibit this general trend, different loci of the journal center are observed for each bearing. For the two axial groove bearing, the journal center moves approximately along a circular arc. With increasing speed, the journal gradually approaches the bearing center because it requires less and less of a convergent wedge to produce 4900 N hydrodynamic force. The pressure dam bearing behaves similar to the plain journal bearing at low speeds. At high speeds, the dam generates significant hydrodynamic pressure that pushes the journal away from the bearing center.

For the tilting pad bearing, the journal center is directly lifted in the vertical direction maintaining very little attitude angle. Such small attitude angles are only possible because of the pads' ability to tilt. Figure 10 shows an example of what occurs when this tilting ability is lost. Here, a noticeable attitude angle was observed when the loaded pad was locked. When this is encountered, it may be attributable to pivot design, operating conditions or even thermocouple or resistance temperature detector (RTD) wire locking the pad in place.

Figure 9 (b) reverses the situation, keeping speed constant and varying load. Like a speed increase, load reduction allows the journal position to reach a lower eccentricity. At 445 N, the journal is almost perfectly centered for both the tilting pad and two axial groove bearings. Once again, because of the dam, the pressure dam bearing maintains a higher eccentricity ratio even at this light loading.

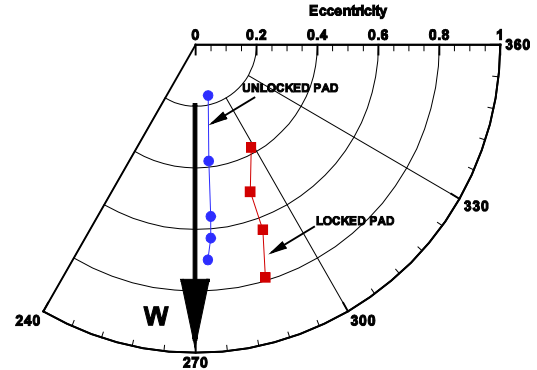


Figure 10. Shaft Centerline test Data for a Tilting Pad Bearing with a Locked and Unlocked Loaded Pad (Courtesy Brechting, 2002)

If the lubricant's viscosity was not allowed to change, the centerline trends in Figure 9(a) and (b) would be identical, i.e. increasing speed and decreasing load would equivalently affect the journal's operating position. This is why the dimensionless Sommerfeld number  $S$ , which combines speed and load effects, was often used to define bearing similarity in early isoviscous studies. The Sommerfeld number is still used today to compare bearings and is typically defined as:

$$S = \frac{\mu\omega}{W_U} \left( \frac{R}{c} \right)^2 \quad (5)$$

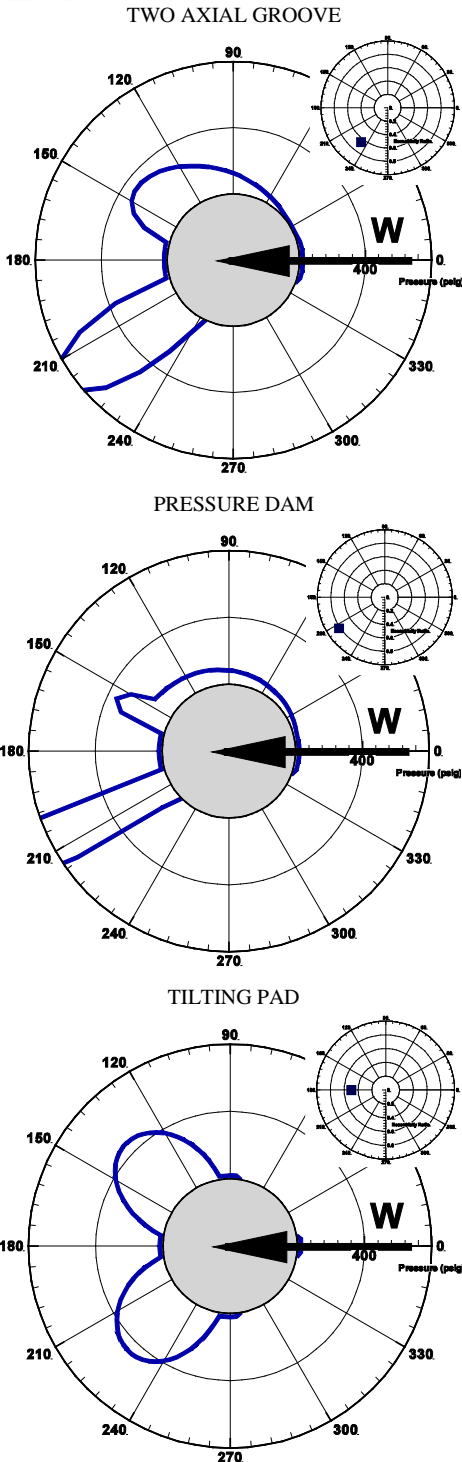


Figure 11. Pressure Distributions with a Horizontal Load ( $W = 4900 \text{ N}$ ,  $N = 7000 \text{ rpm}$ )

One should note that it does not include all geometry factors such as preload or pivot offset. Since thermal and deformation effects are also absent, caution must be used when comparing bearing performance using this rather simplified relationship.

Since the external load is a vector that has direction, journal steady state position is as much dependent on the load's direction as it is on its magnitude. Figure 11 shows the resultant pressure profiles and eccentricity ratios when the 4900 N load is now directed horizontally. Because the load is now pushing towards their axial groove, both fixed geometry bearings' pressure area is dramatically reduced. Likewise, their load capacity is reduced as evidenced by their higher shaft eccentricity ratios. Tower came to the same realization during his experiments. The tilting pad bearing, however, achieves the same eccentricity ratio as before. This can be attributed to its symmetry (four pads equally distributed) and each pad's ability to tilt and generate a load carrying pressure. If the load was directly on pad, one would expect some reduction in load capacity versus the between pad loading (Boyd and Raimondi, 1953; Jones and Martin, 1979).

Load capacity is of great concern in slow roll, turning gear operation with rotational speeds around 10-15 rpm. At such low speeds, the lubricant is unable to generate much supporting pressure, resulting in a very thin film that could be in the regime of boundary lubrication. Compared to hydrodynamic lubrication, the mating surface roughness in boundary lubrication become important and the lubricant film shows increased friction coefficient (Elwell and Booser, 1972; Gardner, 1976). However, since velocity is low and the shaft typically does not vibrate at such low speed, boundary lubrication does not necessarily mean bearing failure. A generally accepted criterion is that the minimum film thickness must be at least twice the surface roughness to insure successful operation.

#### Viscous Shearing and Temperature Rise

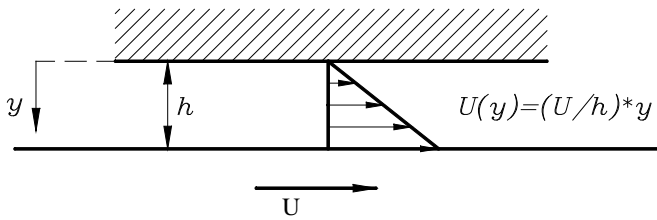
Section summary:

- Viscous shearing causes temperature rise.
- Temperature rise affects bearing performance through lubricant viscosity reduction and solid deformations.
- Shaft speed is the primary operating factor compared to load.

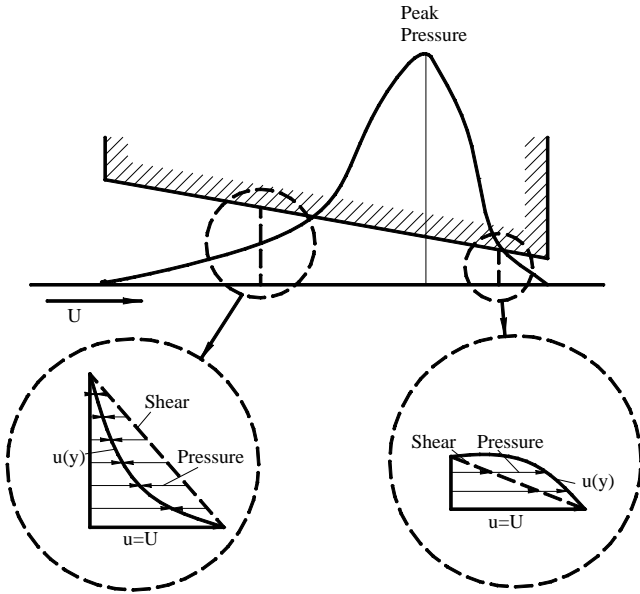
Table 1. Lubricant Viscosity at Different Temperatures

Temperature (°C)	Absolute Viscosity (Centipoise)		
	ISO VG 32	ISO VG 46	ISO VG 68
40	25.86	37.37	55.57
100	4.12	5.30	6.89

While producing load carrying capacity, the lubricant film also generates heat that causes temperature rise in operation. It is well known that a lubricant's viscosity is extremely sensitive to temperature. Table 1 provides some indication for several common turbine oils. Figure 9 has already shown some thermal effects: due to different temperature rises, increasing speed and decreasing load are not equivalent, and the centerline trend in Figure 9(a) differs from that in (b). To fully understand the thermal effects of journal bearings, one must grasp the principle of viscous shearing which is their heat generation mechanism.



(a) Lubricant Shearing Between Parallel Surfaces



(b) Lubricant Flow within a Bearing Convergent Wedge

Figure 12. Shearing Flows in Lubricant Film

Figure 12(a) shows the flow of lubricant being sheared by two parallel surfaces. Since the lubricant adheres to both surfaces, it remains stationary on the upper surface and moves at the same velocity as the lower plate. For laminar flow, layers of lubricant move smoothly and the velocity profile is a straight line. In case of the convergent film within a bearing, Figure 12(b) shows that the actual lubricant flow is a little more complex. Nevertheless, the shearing type flow is still dominant unless the journal eccentricity is very high. This shearing motion creates frictional stresses between the lubricant layers. Per Newton, the fundamental relation for fluid friction (as a stress) takes the form  $\tau = \mu(du/dy)$ . Using the parallel plate model, it can be simplified to  $\tau = \mu U/h$ . Thus, increasing lubricant viscosity or shaft speed increases the viscous shearing and consequently, heat generation. This heat generation due to viscous shearing impacts a bearing's performance in several ways:

- Reduction in lubricant viscosity due to increased temperature
- Thermal growth and distortion of surrounding surfaces affecting the film shape
- Heating of the lubricant and bearing materials toward their thermal failure limits

Figure 13(a) demonstrates the influence of shaft speed on bearing temperature rise. For the two axial groove bearing, as the shaft accelerates from 1000 rpm to 19000 rpm, the peak pad temperature substantially increases from 50 °C (125°F) to 110 °C (230°F), which is near the failure limit. The operating viscosity is consequently reduced according to Table 1. Because of this viscosity reduction, speed increases are less and less effective in producing hydrodynamic pressure to lift the journal. This is apparent in Figure 9(a). Meanwhile, since heavier load results in smaller h on the loaded pad, the external load also affects pad temperature. However, as shown in Figure 13(b), its thermal influence is substantially weaker compared to the shaft speed.

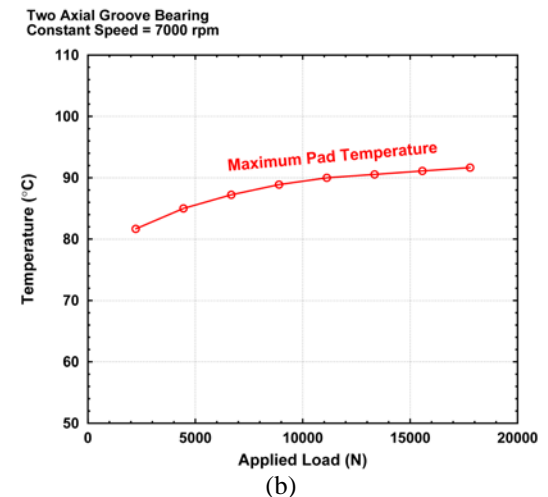
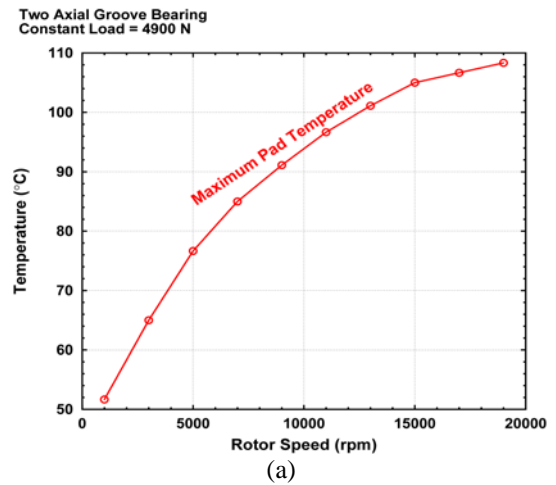
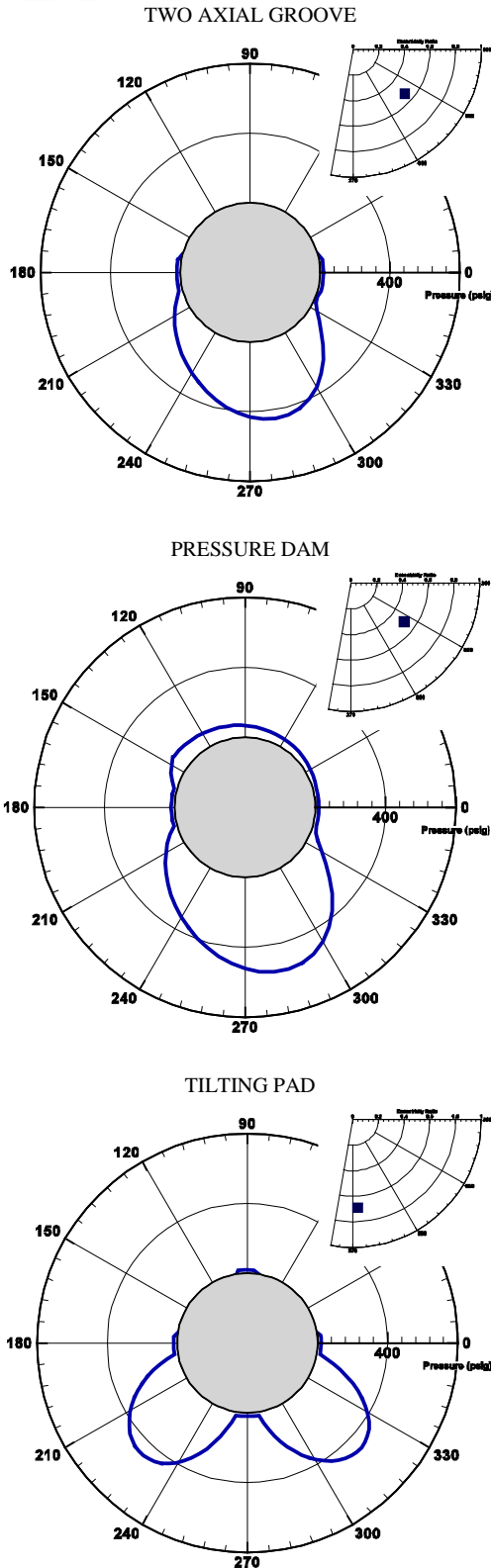


Figure 13. Maximum Pad Temperature versus Speed and Load

Considering the thermal effects on lubricant viscosity, Figure 14 presents pressures and journal positions of the same three bearings under the same operating condition. Compared to the isoviscous results in Figure 8(c), the pressure profiles do not show significant changes because the sums of the pressures must still equal the 4900 N applied load. The thermal effects on load capacity are most evidently shown by the new journal equilibrium positions. The two axial groove bearing's eccentricity ratio has increased from 0.32 to 0.53, and the attitude



angle also decreased by about 10°. For the tilting pad bearing, the journal has moved vertically downward from a position of 0.5 eccentricity ratio to a 0.7 position. The journal position drop is the result of reduced load capacity because of viscosity reduction due to shearing heat generation. It can also be explained as the following: to generate the same force with a less viscous oil, the bottom pad needs to have a smaller clearance and larger wedge ratio  $h_i/h_o$ , which is achieved by the increased journal eccentricity.

*Power Loss*

Section summary:

- Mechanical energy is converted into heat through viscous shearing.
- Shaft speed is the primary operating factor compared to load.

The increased temperature in fluid film is the result of mechanical work done by the shaft. In turn, friction caused by the shaft shearing the lubricant produces a resistive torque on the shaft and consumes mechanical power. This friction loss is closely related to a bearing's size, clearance, shaft speed, and oil viscosity. A bearing's size dictates the area of shearing. Therefore, the partial arc design, which eliminates the top pad of a plain journal bearing, is often used to minimize friction loss (Byrne and Allaire, 1999). As shown in Figure 15, power loss increases with increasing shaft speed. And the partial arc bearing saves noticeable amount of horsepower, especially at high speeds. Directly lubricated bearings are sometimes operated with reduced oil flow to decrease power loss. Similar to the partial arc design, this practice effectively reduces a bearing's shearing area through starvation, which will be discussed later in the modeling section.

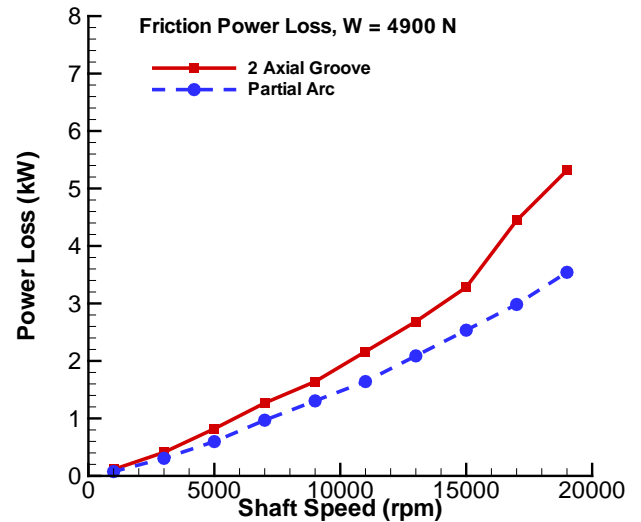


Figure 15. Friction Power Loss versus Shaft Speed

Figure 14. Pressure Distribution Comparison, Variable Viscosity ( $W = 4900\text{ N}$ ,  $N = 7000\text{ rpm}$ )

Petrov (1883) conducted pioneering work on viscous friction and proposed the Petrov's Law which is still used as a quick estimate for bearing power loss. He estimated the frictional



torque according to:

$$T_{\text{friction}} = \frac{2\pi R^2 L \mu U}{c} \quad (6)$$

$$= (2\pi RL) \left[ \mu \left( \frac{U}{c} \right) \right] \cdot R = (\text{Surface Area}) [\text{Shear Stress}] (\text{Moment Arm})$$

Power loss predictions using Petrov's Law turn out to be liberal because the shaft is assumed centered (unloaded) within the bearing clearance. Since a bearing is always loaded statically and dynamically, it has more friction loss according to Figure 13 (b) (temperature rise is the result and indicator of mechanical energy loss). Turbulent flow also increases friction loss due to additional eddy stresses.

### Oil Supply Flowrate

Section summary:

- Oil supply is necessary to maintain steady state operation.
- Housing design (flooded or evacuated) can affect the required flowrate for satisfactory operation.

Another important steady state parameter is the oil supply flowrate that the bearing requires. Lubricant flows into a pad at its leading edge, exiting at its trailing edge and axial ends. Usually, the majority of the oil leaving the trailing edge enters the next pad and continues to circulate inside the bearing (called hot oil carryover). The oil leaving the axial ends is drained out and must be replenished by fresh oil from the lube system. Therefore, one philosophy is that the supply flowrate needs to be at least equal to the bearing's side leakage rate. Using the previous two axial groove bearing as an example, Figure 16 plots the minimum required flow rate as functions of shaft speed and applied load. Since either higher speed or heavier load leads to stronger hydrodynamic pressure, the side leakage, driven by the film pressures, increases as a result.

This philosophy can be applied to determine the minimum required flowrate for bearings using an evacuated housing design that has no end seals. In this case, if the oil supply is insufficient, the bearing will experience starvation, which will be discussed in greater detail in the modeling section later. Although starvation does not mean unacceptable bearing performance, its consequences must be very carefully considered.

In a conventional tilting pad bearing design, end seals are often used, creating an oil sump in which the pads are submerged or flooded. Theoretically, there is no risk of starvation in this situation. However, to avoid high temperature, sufficient oil must be supplied to keep the oil sump reasonably cool. Thus, the flowrate is often determined based on the requirement that temperature rise between the oil supply and drain is below certain recommended limit.

One should bear in mind that lubricant is dragged into the bearing clearance by shaft rotation. Generally, it is not pumped into it by high supply pressure. Therefore, the function of the oil pump is typically to send enough oil into the bearing and keep it circulating. Furthermore, the bearing clearance will accept only

a finite quantity of oil. This amount of oil consumed by the bearing clearance is simply a function of the shaft speed, clearance and minimum film thickness. Therefore, excessive oil supply will not effectively send more oil into the clearance. Instead, it affects the bearing's performance largely by cooling its environment. Methods to determine the supply flowrate and inlet orifice size can be found in Nicholas (1994).

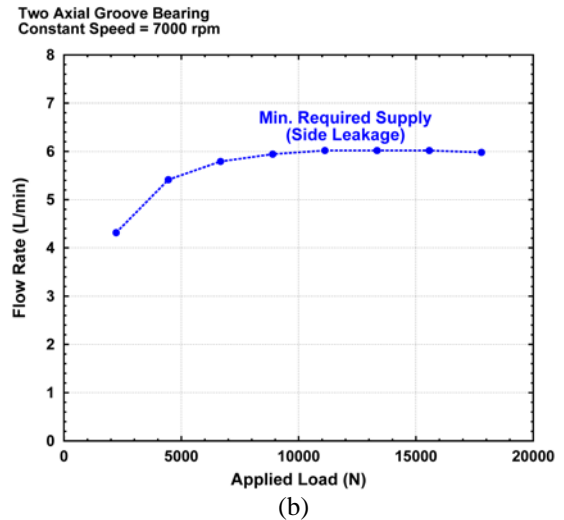
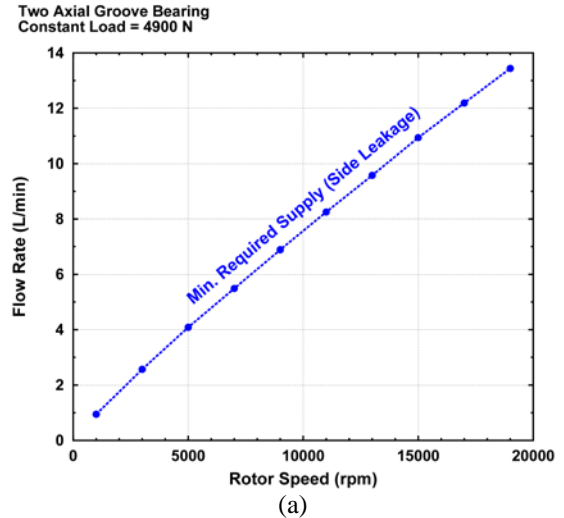


Figure 16. Minimum Required Supply Flow versus Speed and Load

The basic working principles governing the steady state operation of fluid film journal bearings are summarized in Figure 17. A convergent wedge, a moving surface and viscous lubricant are the three ingredients necessary to generate the film hydrodynamic forces to support the applied load. An accompanying phenomenon is viscous shearing that causes temperature rise and power loss. The temperature rise and power loss are related because the energy used to heat up the film is converted from the shaft mechanical energy. Increased temperatures lead to oil viscosity reduction and bearing deformation. In turn, the deformations also change the bearing geometry and thus, the wedge shape.

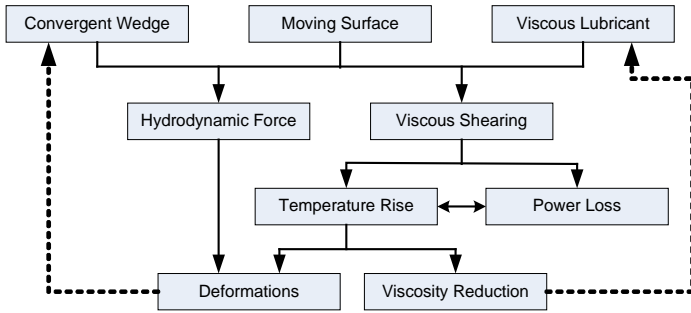


Figure 17. Basic Working Principles for Steady State Operation

### Dynamic Performance

Section summary:

- A bearing is a component of an integrated dynamic system.
- A bearing can be dynamically represented as springs and dampers in a linearized model.
- Stiffness and damping coefficients have significant rotordynamic implications.
- Dynamic coefficients are dependent on shaft speed and applied load.
- There are two categories of self-excited instability related to bearings: oil whirl and shaft whip.

Desirable steady state operation, where the bearing is running with sufficient load capacity and acceptable temperatures, helps to ensure the long term reliability of the bearing itself. However, the bearing's dynamic properties must also be acceptable for the overall machine's reliability. This is because a bearing's dynamic properties, in conjunction with dynamics of the rest of the rotor system, govern all aspects of a machine's vibrational performance.

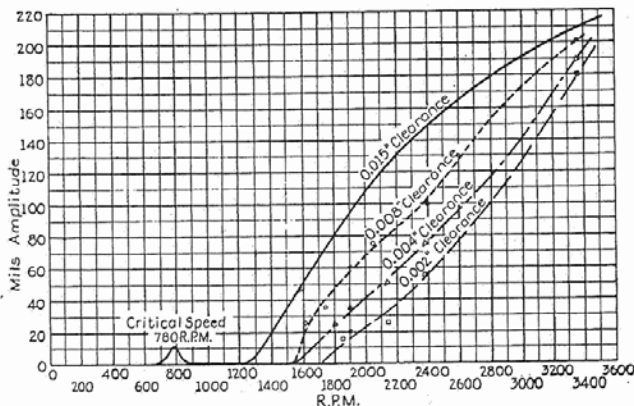


Figure 18. Newkirk and Taylor's Oil Whip Measurements (Courtesy Newkirk and Taylor, 1925)

The dynamic performance of journal bearings first came under scrutiny because of the vibration problems encountered by Newkirk and Taylor (1925). In this landmark paper, Newkirk and Taylor describe the first published account of a rotor going

unstable due to "oil whip." Initially, they thought the vibration was caused by improper shrink fits which were the only known source of whipping instability (Newkirk, 1924). They eventually found that the bearing's parameters such as clearance (Figure 18), loading, alignment and oil supply (in some tests, the supply was cut off!!) controlled the instability.

With the considerable development of steam turbine technology, the 1920s continued to provide evidence that a machine's vibration was heavily linked to the operation of the bearings. In two papers, Stodola (1925) and one of his pupils, Hummel (1926), introduced the concept that a bearing's oil film dynamically acts like a spring. They found that, when this oil spring's stiffness was considered, their rotor critical speed calculations could be improved (Lund, 1987). They also realized that the oil film stiffness could be very non-linear, i.e., the film force variation was not directly proportional to the journal position variation. While many continue to study this non-linear complication, most of the machines in operation today were designed using *linearized* stiffness and damping properties for the oil film.

As shown in Figure 19, the fluid film can be represented by springs and dampers. The static load  $W$ , such as gravity, establishes the journal's steady state equilibrium position. Then, some dynamic force, such as rotor unbalance forces, pushes the journal away from its equilibrium and causes it to whirl on an elliptical orbit (Figure 20). To have an acceptable vibration level, the orbit's size must be relatively small compared to the bearing clearance. When this is the situation, the vibration is said to be in the linear range and the film dynamic forces are directly proportional to the displacements ( $\Delta x$ ,  $\Delta y$ ) and associated whirling velocities ( $\Delta \dot{x}$ ,  $\Delta \dot{y}$ ). This relationship is given by:

$$\begin{Bmatrix} F_x \\ F_y \end{Bmatrix} = - \begin{bmatrix} K_{xx} & K_{xy} \\ K_{yx} & K_{yy} \end{bmatrix} \begin{Bmatrix} \Delta x \\ \Delta y \end{Bmatrix} - \begin{bmatrix} C_{xx} & C_{xy} \\ C_{yx} & C_{yy} \end{bmatrix} \begin{Bmatrix} \Delta \dot{x} \\ \Delta \dot{y} \end{Bmatrix} \quad (7)$$

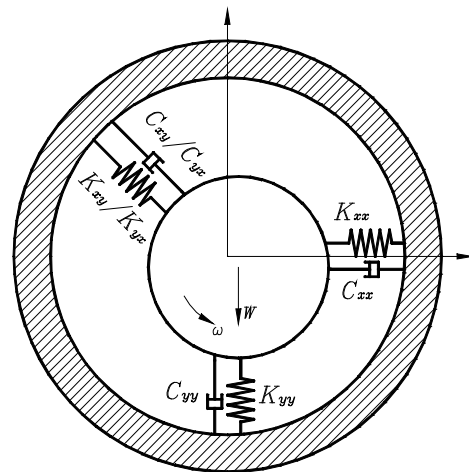


Figure 19. Dynamic Properties of the Fluid Film

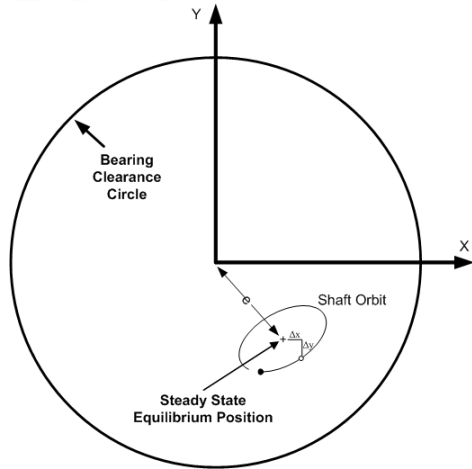


Figure 20. Journal Steady State Position and Orbit

Where the  $K_{ij}$  and  $C_{ij}$  are called linearized stiffness and damping coefficients, respectively. In other words, at an instantaneous journal position, the horizontal and vertical dynamic forces due to the oil film can be obtained by expanding Equation (7):

$$\begin{aligned} F_x &= -(K_{xx} \Delta x + K_{xy} \Delta y + C_{xx} \Delta \dot{x} + C_{xy} \Delta \dot{y}) \\ F_y &= -(K_{yy} \Delta y + K_{yx} \Delta x + C_{yy} \Delta \dot{y} + C_{yx} \Delta \dot{x}) \end{aligned} \quad (8)$$

where the negative sign implies that the force is acting on the rotor.

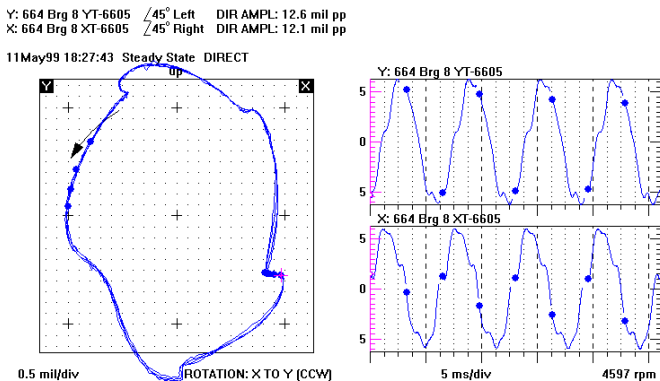


Figure 21. Unstable Rotor Exhibiting Large Vibration

To justify the use of linearized dynamic properties, one should understand the other situation where the vibration levels are relatively large. Figure 21 shows the classic example of an unstable shaft where the orbit nearly fills up the entire bearing clearance. Here the rotor has almost reached the so-called “limit cycle.” Since this motion is large relative to the bearing clearance, linearized coefficients are inadequate to represent the film dynamic forces. Therefore, they cannot be used to predict the actual amplitudes and forces for such large vibrations. However, the strength of the linearized coefficients is their ability to predict whether or not such unstable vibrations will

occur. This ability, combined with their accuracy in predicting vibration amplitudes within the range of interest [up to 40% of the clearance according to Lund (1987)], enables modern rotordynamics to be firmly based on their use.

Now, let us define and explain those linearized dynamic coefficients in Equations (7) and (8). The following two stiffness coefficients are called principal or direct coefficients:

$$K_{xx} = -\Delta F_x / \Delta x \quad \text{Horizontal principle stiffness} \quad (9)$$

$$K_{yy} = -\Delta F_y / \Delta y \quad \text{Vertical principle stiffness}$$

where each relates the change in force in one direction due to a displacement in the same direction. In other words, these direct stiffnesses provide a restoring force that pushes the journal back toward its steady state equilibrium position. As shown in Figure 22(a), a positive horizontal perturbation  $\Delta x$  generates a negative horizontal force  $F_{xx} = -K_{xx}(\Delta x)$ , a negative vertical perturbation  $-\Delta y$  yields a positive vertical force  $F_{yy} = -K_{yy}(-\Delta y)$ . The combination is a radial force that tries to push the journal back to  $O_s$ .

The principal stiffnesses are extremely important with respect to the machine’s vibration performance. Their magnitude, relative to the shaft stiffness, governs the location and amplification of the rotor’s critical speeds. They are equally important for stability purposes. Large asymmetry of  $K_{xx}$  and  $K_{yy}$  is the main cause for split critical speeds (API 684, 2005) and non-circular (elliptical) orbit shapes. Although such asymmetry can be very beneficial with respect to stability (Nicholas et al., 1978), symmetry of these coefficients is usually preferred for unbalance response considerations.

Two principal or direct damping coefficients are also present:

$$C_{xx} = -\Delta F_x / \Delta \dot{x} \quad \text{Horizontal principle damping} \quad (10)$$

$$C_{yy} = -\Delta F_y / \Delta \dot{y} \quad \text{Vertical principle damping}$$

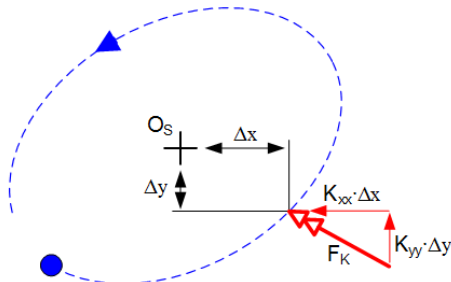
Here the damping coefficients relate the change in force due to a small translational velocity. Because of the rotor’s whirling motion, the combination of these two principal damping coefficients produces a force that is tangential to the vibration orbit. Furthermore, as shown in Figure 22(b), this direct damping force acts against the whirling motion, helping to retard or slow it.

Like their direct stiffness counterparts, the principal damping terms dictate much about the machine’s unbalance response and stability. They are often the predominant source of damping in the entire machine. However, their effectiveness in reducing critical speed amplification factors and preventing subsynchronous instabilities is determined also by the bearing’s direct stiffness coefficients as well as the shaft stiffness. For the direct damping to be effective, the bearing cannot be overly stiff because the damping force relies on journal’s squeeze motion. Also, contrary to one’s initial instincts, large amounts of

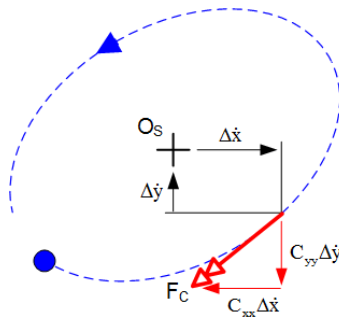
damping can actually be detrimental. Barrett et al. (1978), in an important fundamental paper, highlighted this fact and verified that the optimum amount of bearing damping is a function of the bearing (direct) and shaft stiffnesses.

$$K_{xy} = -\Delta F_x / \Delta y \quad (11)$$

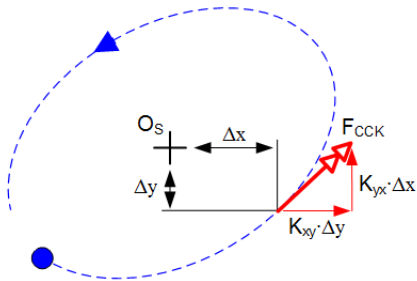
$$K_{yx} = -\Delta F_y / \Delta x$$



a) DIRECT STIFFNESS FORCE



b) DIRECT DAMPING FORCE



c) CROSS COUPLED STIFFNESS FORCE

Figure 22. Dynamic Forces in the Fluid Film

The off-diagonal stiffness coefficients in Equation (7),  $K_{xy}$  and  $K_{yx}$ , are the infamous cross-coupled stiffness coefficients. The meaning of cross coupled becomes apparent when these stiffnesses are defined as:

As an example, the coefficient  $K_{yx}$  relates a vertical force due to a horizontal displacement. Thus, the horizontal and vertical directions have become coupled. This exactly corresponds to the behavior we highlighted in Figure 8 for the two fixed geometry bearing, where a displacement in one direction resulted in force component perpendicular to this displacement.

Almost all structures have such cross-coupled stiffness terms but most are symmetric in nature where  $K_{xy} = K_{yx}$ . Rotor systems are unique in that this symmetry usually does not exist ( $K_{xy} \neq K_{yx}$  and usually  $K_{xy} > 0$ ,  $K_{yx} < 0$ ). Fundamentally, their presence and their asymmetry result from the various fluids rotating within a turbomachine, such as oil in bearings and gas in labyrinth seals. Figure 22(c) illustrates why asymmetric cross-coupled stiffnesses are detrimental. Instead of opposing the rotor's whirling motion like the direct damping, the cross-coupled stiffnesses combine to create a force pointing in the whirl direction, promoting the shaft vibration.

When the direct damping force is unable to dissipate the energy injected by the cross-coupled stiffness force, the natural frequency (typically the lowest one with forward whirling direction) will become unstable, causing the shaft to whirl at this frequency (Ehrich and Childs, 1984). This frequency will appear in the vibration spectrum, typically as a subsynchronous component. Such self-excited vibration is the reason why these cross-coupling coefficients are of such concern for stability purposes.

Unlike their fixed geometry counterparts, tilting pad bearings produce very little cross-coupled stiffness, which explains their popularity. This fact was actually touched on earlier in Figures 8 and 9 where the tilting pad bearing's journal position moved only vertically under a vertical load. It consistently maintains a small attitude angle, indicating small amount of cross-coupled stiffness present. As shown in Figure 9, the attitude angle of the two fixed geometry bearings approaches 90 degree at light loads, implying the cross-coupled stiffnesses are very large relative to their direct counterparts. Thus, instability is often encountered when running fixed geometry bearings at light loads.

Like the steady state performance, the dynamic coefficients vary with shaft speed and external load. Figure 23 shows the two axial groove bearing's coefficients as functions of the shaft speed. The vertical stiffness  $K_{yy}$  and damping  $C_{yy}$  decrease significantly as the speed increases from 1000 to 10000 rpm. Meanwhile, the bearing becomes less stable because it loses considerable damping while retaining a high cross-coupled stiffness. Therefore, an unbalance response analysis must include the coefficients' speed variations for accurate prediction of critical speeds and vibration levels. Such speed dependency is also the reason why the amplification factor of the first critical speed should not be used as a measure of stability for higher speeds like maximum continuous speed.



Two Axial Groove Bearing  
Constant Load = 4900 N

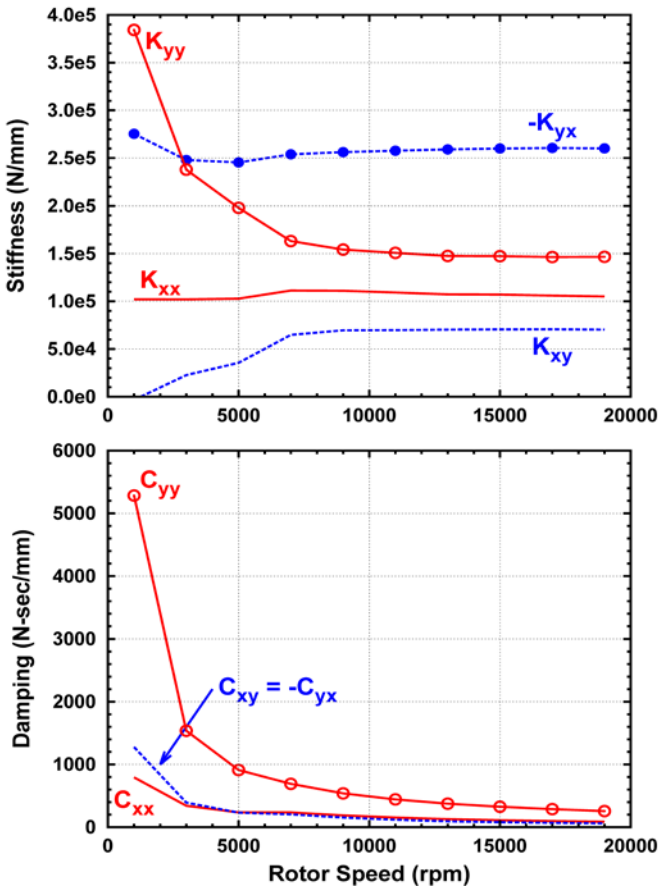


Figure 23. Two Axial Groove Bearing Dynamic Coefficients versus Speed

The stabilities of the plain journal and pressure dam bearings are compared in Figure 24. The tilting pad bearing is not presented because its stability is not an issue. Here, stability is measured by the rigid rotor threshold speed, which is largely dependent on the bearing properties and loading (Lund and Saibel, 1967). As shown in Figure 24, the bearing is predicted to be unstable at around 10000 rpm using the bearing coefficients at 700 rpm; using the coefficients at 10000 rpm, instability is predicted at approximately 7600 rpm. Therefore, a rigid rotor would go unstable at approximately 7600 rpm where the curve intersects the 1x line. The pressure dam bearing shows improved stability since the intersection is beyond 10000 rpm. Experimental results and more discussions can be found in Lanes, et al. (1981) and Zuck and Flack (1986).

Examining all the ways a bearing's dynamic properties can influence a machine's rotordynamics is beyond the scope of this tutorial. The literature on the subject is extensive and the student is encouraged to examine API 684 (2005) for further explanation and references. Fundamentally, a machine's rotordynamic performance becomes an interplay of how the dynamics of various components (bearings, shaft, seals, supports, etc.) interact when combined together as a *system*. In other words, the

overall dynamic performance is governed by the system, not one particular component in general.

Oil whirl is one exception where the bearing's dynamic properties dominate the rotordynamic behavior of the system. First observed by Newkirk and Taylor (1925) who called it "journal whirl," this instability phenomenon has received considerable interest even though its occurrence is rare in most machinery applications. Some exceptions are gearboxes and internally geared compressors operating at low power and resulting in small gear forces.

As shown in Figure 25, the frequency of the system's first forward mode follows the 0.5x line at low shaft speeds. When the system becomes unstable at such low speed, the frequency of the subsynchronous vibration equals half of the running speed and *tracks* it as the rotor accelerates. Since the shaft does not experience much bending, it can be regarded as a rigid body or just a mass inside the bearing. Therefore, the oil whirl instability is dominated by the dynamic properties of the bearing. With increasing shaft speed, the unstable mode steps into the territory of shaft whip where the subsynchronous frequency is locked at a constant value. Unlike oil whirl, the rotor's mode shape in whip undergoes noticeable bending and its flexibility plays a significant role in the system's overall dynamics.

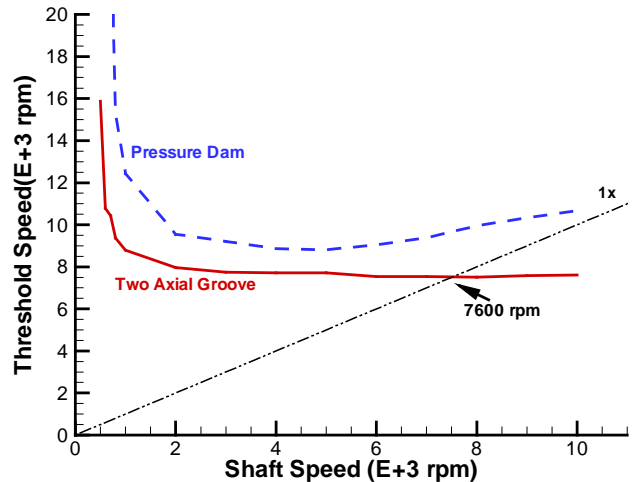


Figure 24. Rigid Rotor Stability Threshold Speeds versus Shaft Speed

In real life, most unstable machines exhibit shaft whip directly without exhibiting oil whirl behavior. To produce the 0.5x oil whirl, the bearing must be unloaded, allowing it to operate at very low eccentricity. Hamrock (1994) theoretically deduced that oil whirl would occur if the bearing had a constant pressure (zero) throughout the film. Obviously, a constant (zero) pressure can only be achieved with a centered or unloaded shaft. The unloading may be caused by the lack of gravity load like Newkirk and Taylor's vertical rotor (1925), the use of some "centering device" (Muszynska and Bently, 1995), misalignment, overhung mass effects, or the presence of external forces from gearing or partial arc steam admission forces which

can negate the gravity loading. Again, oil whirl is driven by large bearing cross coupling, and thus occurs only with fixed geometry bearings.

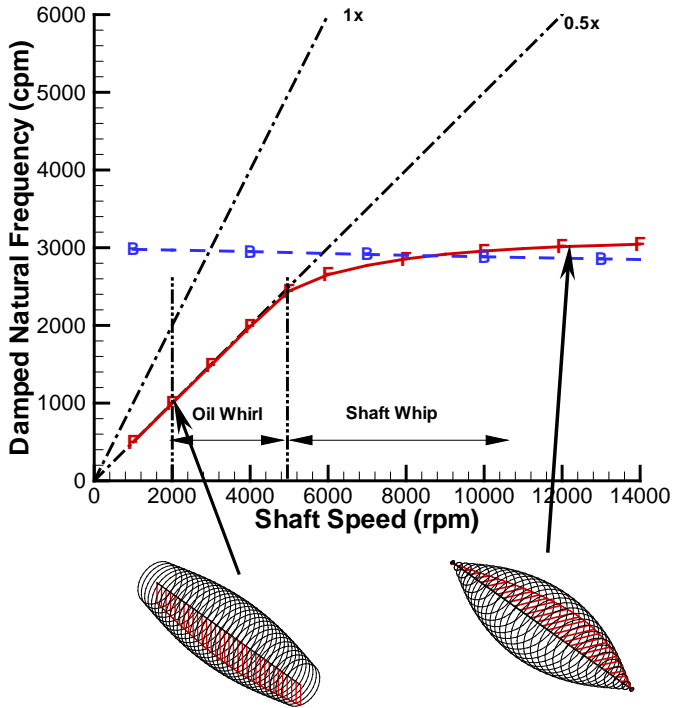


Figure 25. Campbell Diagram Showing Oil Whirl and Shaft Whip

## MODELING

Accurate evaluation of a bearing's performance has become a vital factor in the design, operation and troubleshooting of rotating machinery. A number of computer programs have been developed to accomplish this task. This section presents the major aspects of bearing modeling, the mainstream techniques used in those computer codes as well as their potential limitations. First, the general areas that are required in most modern bearing analysis will be covered. Such areas include

- Hydrodynamic pressure
- Temperature
- Deformations
- Turbulence
- Dynamic coefficients

The next step is to assemble those components into a functional computer algorithm. Then, our discussion will switch to special situations such as direct lubrication and starvation. Some modeling difficulties and challenges will be addressed at the end. The objective is to shed some light on those computer tools, and thus, help engineers to use them properly.

### Hydrodynamic Pressure

Section summary:

- Hydrodynamic pressure is the primary physical phenomenon to model.
- The Reynolds equation is the governing equation for thin lubricant film.

Hydrodynamic pressure modeling is the foundation of an accurate bearing analysis. In general fluid dynamics, the film's pressure and velocity distributions are governed by the coupled continuity equation and the momentum equations. The continuity equation comes from the basic law of mass conservation. Each of the three momentum equations, known as Navier-Stokes equations for incompressible flow, is essentially Newton's second law in each direction of the three-dimensional space. Thus, a simple theoretical analysis requires simultaneous solution of four equations, which is not trivial because iterations must be employed and the momentum equations are non-linear. If other parameters such as temperature and turbulence are considered, more equations must be added to the formulation and the solution procedure quickly becomes very complex. Fortunately, such a procedure can be avoided in a bearing analysis and the hydrodynamic pressure can be directly calculated from the following linear equation.

$$\underbrace{\frac{\partial}{\partial x} \left( \frac{h^3}{12\mu} \frac{\partial p}{\partial x} \right)}_{x \text{ Pressure}} + \underbrace{\frac{\partial}{\partial z} \left( \frac{h^3}{12\mu} \frac{\partial p}{\partial z} \right)}_{z \text{ Pressure}} = \underbrace{\frac{U}{2} \frac{\partial h}{\partial x}}_{\text{Shear}} + \underbrace{\frac{\partial h}{\partial t}}_{\text{Squeeze}} \quad (12)$$

Equation (12) is the classic Reynolds equation (Reynolds, 1886). During its derivation, several assumptions must be made: most of all, the fact that the film thickness is much smaller than the bearing's diameter (the typical c/D ratio is on the order of  $10^{-3}$ ). Consequently, the momentum equations can be significantly simplified by neglecting the small terms. From these simplified equations, the pressure across the film is shown to be constant and the velocity components can be directly solved. Then, the Reynolds equation is obtained by substituting the velocity components into the continuity equation and integrating across the film (Szeri, 1979). This classic Reynolds equation also assumes that viscosity is invariant across the film and the flow is laminar. However, Equation (12) can be made more general by relaxing these two conditions (Constantinescu, 1959; Dowson, 1962).

The left hand side of Equation (12) includes the pressure flow terms that represent the net flowrate due to pressure gradients within the lubricant area; the shear flow term on the right hand side describes the net entraining flowrate due to the surface velocity. In steady state, there is no shaft translational motion and the squeeze term  $\partial h/\partial t=0$ . If the shaft is stationary ( $U=0$ ), the right hand side equals zero and no lubricant can enter the bearing clearance. The pressure gradients on the left hand side must be zero to satisfy the flow continuity. Similarly, if the pairing surfaces are parallel ( $\partial h/\partial x=0$ ), the right hand side also

becomes zero and no hydrodynamic pressure can be developed. Therefore, it is shown from the Reynolds equation that the rotating shaft and convergent wedge are the necessary conditions to generate hydrodynamic pressure in steady state. If the clearance is divergent ( $\partial h/\partial x > 0$ ), the Reynolds equation will give artificially negative pressure. However, since the lubricant cannot expand to fill the increasing space, cavitation occurs in this region and the divergent clearance is occupied by streamlets and air-liquid mixture (Heshmat, 1991).

The squeeze term on the right hand side represents the shaft translational motion due to vibration. When the shaft is approaching a pad's surface ( $\partial h/\partial t < 0$ ), the fluid film in between is squeezed and its volume is reduced. Consequently, some lubricant is driven out of the clearance to satisfy flow continuity. According to Equation (12), non-zero  $\partial h/\partial t$  leads to pressure flow on the left hand side. This means hydrodynamic pressure is generated, pushing lubricant out of the thin film.

Figure 26 shows a two axial groove bearing and the bottom pad pressure distribution solved from the steady state Reynolds equation. Hydrodynamic pressure is smoothly developed in the area of convergent clearance. Axially, the pressure distribution is symmetric about the mid-plane and goes down to the ambient pressure at the edges. No hydrodynamic pressure is generated in the cavitated region that exists near the trailing edge of the bottom pad and on the entire top pad.

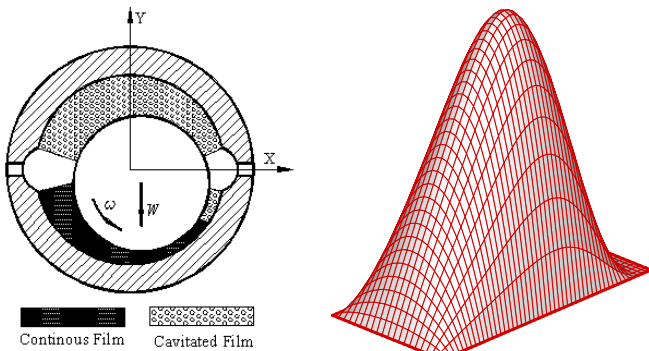


Figure 26. Pressure Distribution on the Bottom Pad of a Two-Axial Groove Bearing

### Temperature

Section summary:

- Including temperature effects is critical for accurate bearing performance predictions.
- The modeling involves shaft, fluid film and bearing pads.
- Energy equation is the governing equation.

One early idea to model the thermal effects is the approach of effective viscosity (Raimondi and Boyd, 1958). This method employs an empirical equation to calculate an effective temperature. From the effective temperature, an effective viscosity is determined and used in the Reynolds equation. While this simple idea recognizes the viscosity reduction due to temperature rise, its effectiveness is very limited and it fails to

give the maximum pad temperature, which is an important operation parameter.

To accurately model the thermal effects, the temperature distribution must be solved from the governing energy equation. Similar to the momentum equations, the energy equation for bearing analysis has been substantially simplified because of small film thickness. The three-dimensional energy equation for laminar flow is usually written in the form of

$$\underbrace{\rho C_p \left( u \frac{\partial T}{\partial x} + v \frac{\partial T}{\partial y} + w \frac{\partial T}{\partial z} \right)}_{\text{Convection}} = \underbrace{\frac{\partial}{\partial x} \left( k \frac{\partial T}{\partial x} \right) + \frac{\partial}{\partial y} \left( k \frac{\partial T}{\partial y} \right) + \frac{\partial}{\partial z} \left( k \frac{\partial T}{\partial z} \right)}_{\text{Conduction}} + \underbrace{\mu \left[ \left( \frac{\partial u}{\partial y} \right)^2 + \left( \frac{\partial w}{\partial y} \right)^2 \right]}_{\text{Dissipation}} \quad (13)$$

As shown in Equation (13), the steady state temperature is determined by three terms. The dissipation term describes the internal heat generation due to viscous shearing. As would be expected, the heating intensity is shown to be proportional to the lubricant viscosity. The heat convection term describes the rate of heat transfer due to the lubricant's motion. And the conduction term determines the heat transfer between the lubricant and surrounding surfaces. It can be shown by dimensional analysis that the heat convection term is usually much larger than the conduction term. Thus, the film physically constitutes a heat source; while some of that heat is conducted away through the solid surfaces, the majority of it is carried away by the flowing lubricant.

To achieve better computational efficiency, two simplified forms of Equation (13) are often used in practice. The first one is the adiabatic equation that is obtained by neglecting the conduction term in Equation (13). The adiabatic energy equation was derived by Cope (1949) and has been widely used for many years. It implies that no heat is transferred to the solids and the film temperature is constant radially. Figure 27 shows the typical adiabatic temperature solution for a smooth pad that has convergent-divergent clearance. Most of the temperature rise takes place in the convergent clearance section where significant viscous shearing occurs. In the divergent region, the temperature rise is significantly reduced due to weak heat generation in the two phase, air-lubricant mixture. Axially, the temperature is almost invariant, showing only slight increase at the edges.

For many years, bearing designers had used adiabatic theory and isoviscous theory to bracket a bearing's actual performance. However, this notion was later invalidated by a number of studies. It became clear in 1960s that the radial temperature variation must be taken into account for accurate bearing modeling (McCallion et al., 1970; Seireg and Ezzat, 1973; Dowson and Hudson, 1963). Moreover, in machinery, such as steam turbines, where a hot shaft conducts heat into the film, the adiabatic assumption is clearly inappropriate. Therefore, another form of the simplified energy equation, which includes the radial heat conduction, has become more popular in modern bearing analysis. Assuming the temperature varies little in the axial

direction, as suggested in Figure 27, the axial heat transfer can be eliminated ( $\partial T/\partial z=0$ ) and the original three-dimensional energy equation is reduced to two-dimensional. As shown in Figure 28, this two-dimensional equation solves the temperature on x-y plane, which is perpendicular to that of the adiabatic energy equation and the Reynolds equation.

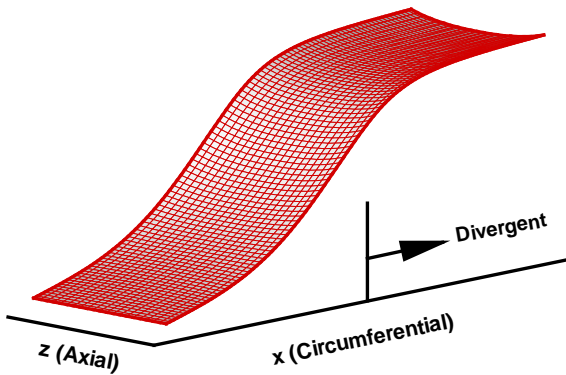


Figure 27. Adiabatic Temperature Solution for a Convergent-Divergent Film

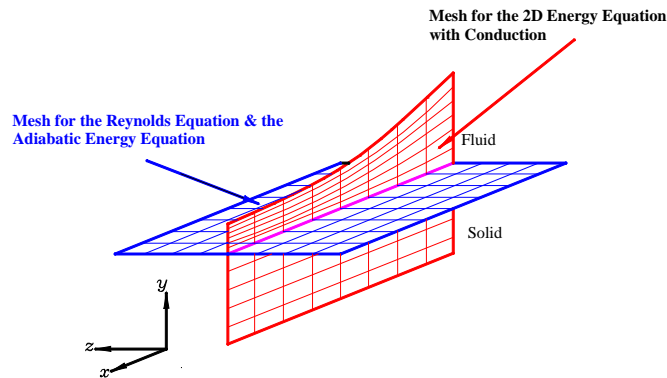


Figure 28. Numerical Meshes for the Governing Equations

Figure 29 presents the temperature contour obtained from this two-dimensional energy equation. The lower rectangular section is the bearing pad and the upper section is the fluid film. For better visualization, the film thickness is enlarged 1000 times and the pad-film interface is highlighted by a bold line. The convergent-divergent clearance is clearly shown on the upper boundary. In the circumferential direction, the film and pad temperatures increase from the leading edge, arrive at the maximum value around the minimum film thickness location, and decrease near the trailing edge as the result of heat conduction. The radial temperature variation is shown to be significant with a hot spot close to the pad surface. This trend is generally true for most bearings regardless of the specific contour values in this example.

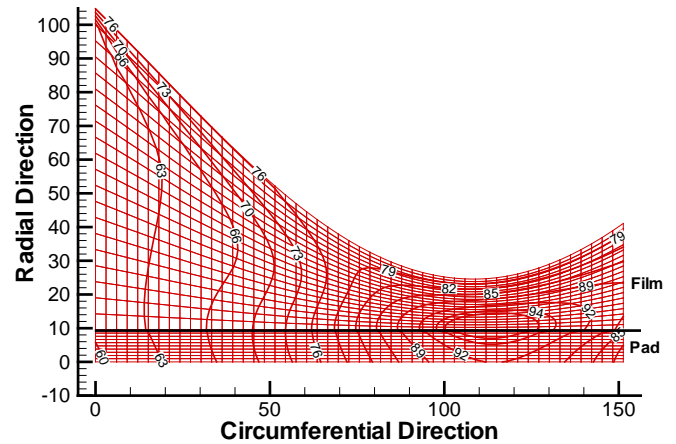


Figure 29. Temperature Contour from the 2-D Energy Equation with Conduction

In some situations, neither radial nor axial temperature profile can be assumed constant and the full three-dimensional energy equation must be solved. For example, in a pressure dam bearing, the temperature inside the pocket is much lower than that in the land regions (He et al., 2004). Or if the bearing is misaligned with respect to the shaft, the temperature is higher at one axial edge where the film thickness is minimum.

Most theoretical algorithms solve one form of the energy equation or another. Usually, the Reynolds equation is solved first using assumed lubricant viscosity. After the pressure distribution is obtained, the velocity components can be derived and the energy equation is solved to give the temperature distribution. Then, the viscosity is recalculated and the Reynolds equation is solved again using the updated viscosity. This procedure continues till the difference between two consecutive iterations is sufficiently small.

One may have noticed that the energy equation does not directly govern the temperature in the solid pad. One way to obtain the pad temperature is to solve a separate heat conduction equation. Since the temperature and heat flux must be continuous at the film-pad interface, the heat conduction equation is coupled with the energy equation and they can be solved through iterations. The second approach is to extend the energy equation into the solid pad. In the fluid film, the energy equation has the convection, conduction and dissipation terms. In the solid pad, convection and dissipation terms are set to zero, leaving the heat conduction equation. In order to satisfy the heat flux continuity, harmonic averaging is employed to modify the heat conductivity on the film-pad interface (Paranjpe and Han, 1994).

The thermal effects on the predicted bearing performance are demonstrated through the example of a two axial groove bearing reported in Fitzgerald and Neal (1992). All thermohydrodynamic (THD) results are calculated using the two-dimensional energy equation including heat conduction. Figure 30 compares the pad surface temperatures along the axial centerline. The theoretical results have close agreement with the experimental data. Figure 31 shows the journal eccentricity ratio under various loads and speeds. The THD analysis consistently

gives more accurate results compared to the isoviscous hydrodynamic (HD) analysis, especially in the case of 8000 rpm that has relatively high temperature rise. The predicted vertical stiffness coefficients  $K_{yy}$  are plotted in Figure 32. The difference due to the inclusion of the thermal effects can be as much as 30 percent at high speeds.

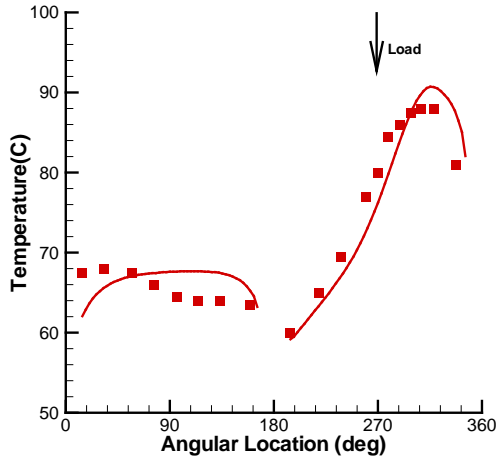


Figure 30. Pad Surface Temperature Comparison,  $L/D=0.5$ ,  $N=8000$  rpm,  $W=5.43$  KN (Experimental Results from Fitzgerald and Neal, 1992)

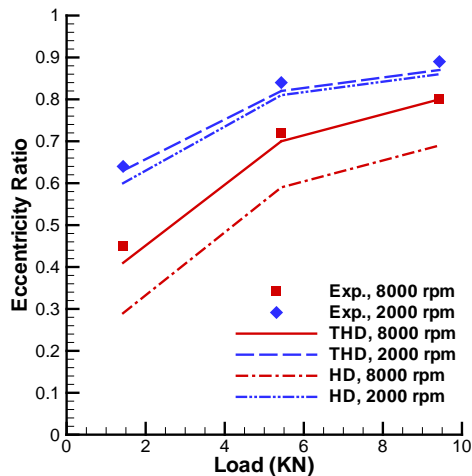


Figure 31. Thermal Effects on the Predicted Eccentricity Ratio (Experimental Results from Fitzgerald and Neal, 1992)

### Deformations

Section summary:

- Elasticity modeling has become more and more important as a result of increasing high speed, heavy load applications.
- It involves deformations of bearing pad, pivot, shaft and shell. Theoretical models require caution in their use.

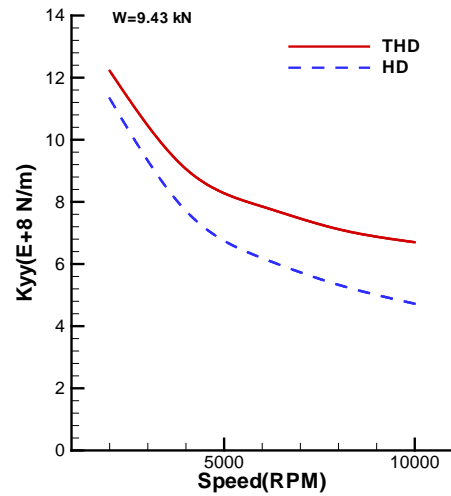


Figure 32. Thermal Effects on the Predicted Direct Stiffness

Deformations change a bearing's operating geometry, and, consequently, affect all aspects of a bearing's performance. Because of its flexible assembly, a tilting pad under high speed and/or heavy load is subject to deformations that are composed of two parts: mechanical deformation due to pressure and thermal deformation due to temperature rise. The simplest elastic model treats a tilting pad as a one-dimensional curved beam (Ettles, 1980; Lund and Pedersen, 1987). If the deformed pad is assumed circular, the clearance variation  $\Delta C$  can be calculated and the bearing is modeled with a modified clearance  $c=c_0+\Delta c$ . Alternatively, the beam equation can be numerically integrated and the nodal displacements are used to correct the film thickness.

A more advanced approach is to formulate the problem based on the principle of virtual work and solve it using the finite differences or finite element method (Brugier and Pascal, 1989; Desbordes et al., 1994). Although the actual pad is three-dimensional, a two-dimensional plain strain approximation is often used since the deformations are primarily on the x-y plane. Figures 33 (a) shows the shape of a tilting pad under mechanical deformation. The finite element grid before deformation is plotted with the dashed red lines and the deformed pad is plotted with the solid blue lines. The mechanical deformation is shown to be mainly in the radial direction. Since the displacements around the pivot are smaller than those near the ends, mechanical deformation effectively increases more  $c_p$  than  $c_b$ . Consequently, the pad preload,  $m$ , may increase or decrease depending on the relative  $c_p$  and  $c_b$  variations. Figure 33 (b) shows the pad deformations under both mechanical and thermal loads. Since the thermal deformation is dominant in this example, the total deformation is shown as largely thermal growth with decreased  $c_b$  and  $c_p$ . The pad preload also varies because the temperature rise is not uniform and the pivot constrains the deformations near the pad center. In this particular example, the mechanical load had little effect on the preload, while the thermal deformation increases it.

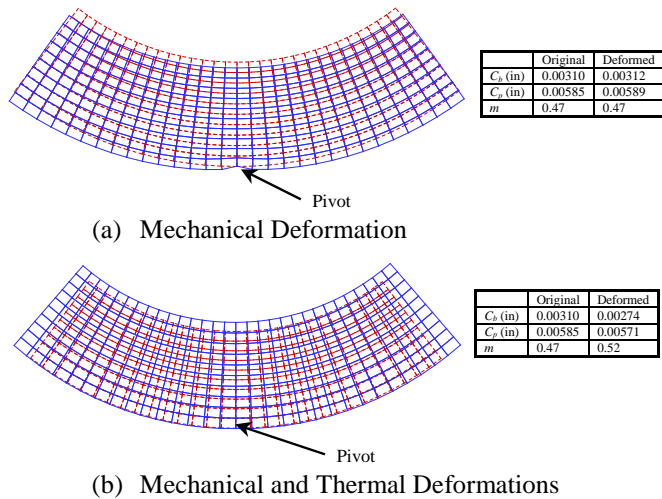


Figure 33. Pad Deformations Obtained by 2-D Finite Element Method

In addition to the pad deformations, the journal and bearing shell also experience thermal growth in operation. Due to the rotation, the journal temperature is usually assumed constant and its deformation is modeled as free thermal growth at uniform temperature (Kim et al., 1994). The bearing outer shell can also be modeled in a similar fashion. In addition, the pivot deformation under heavy mechanical load can be calculated from the Hertzian contact theory (Kirk and Reedy, 1988; Nicholas and Wygant, 1995).

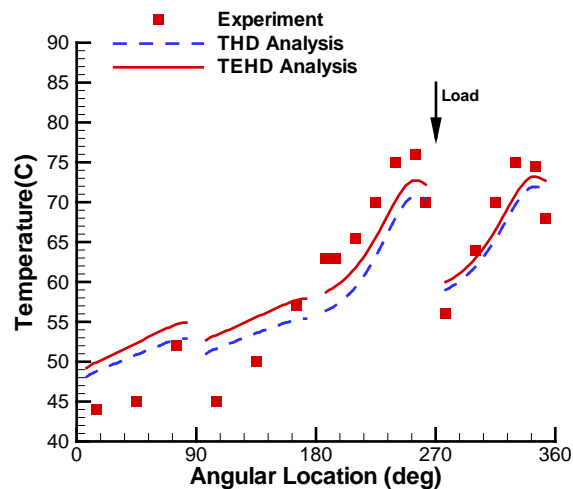


Figure 34. Elastic Effects on the Pad Temperature Calculations (Experimental Results from Fillon et al, 1992)

Figure 34 presents the temperature predictions of a four-pad tilting pad bearing experimentally investigated by Fillon et al. (1992). The thermoelastohydrodynamic (TEHD) analysis takes into account both the thermal and elastic effects. As shown in this figure, the inclusion of deformations brings the theoretical results closer to the experimental data. While this example shows that the inclusion of elasticity can improve the predictions, the

deformation models, especially the journal and shell models, must be used very carefully. In fact, it is often inadequate to model the journal and shell thermal growth as free expansions. Since the journal is part of the entire shaft, its growth is not “free” and its proper modeling requires the knowledge of the entire shaft temperature distribution. Meanwhile, the bearing shell often cannot expand freely either, because it is constrained by the bearing housing. Its deformation is significantly affected by the housing conditions, including its stiffness, temperature, and shrink fit interference. A poor evaluation of the journal and shell deformations can introduce very large errors in the modeling predictions. Although the fundamental physics seem straightforward, accurate modeling of elasticity is one of the most difficult tasks in a bearing analysis.

### Turbulence

Section summary:

- Turbulent bearings have different behaviors compared to laminar bearings.
- The turbulence effects must be included in modeling.

Fluid film bearings may operate in different flow regimes: laminar, transitional or fully developed turbulent. In laminar flow, the fluid particles are moving in layers with one layer gliding smoothly over the adjacent layers. In turbulent flow, the fluid particles have irregular motion and the flow properties, such as pressure and velocity, show erratic fluctuations with time and with position. Since it is impossible to track the instantaneous flow properties, their statistical mean values are sought in a turbulent flow calculation. The flow regime is usually indicated by the Reynolds number defined as  $Re = \rho U h / \mu$ . The flow is laminar at low Reynolds numbers. As  $Re$  increases, the flow becomes unstable and partially turbulent, and eventually evolves into full turbulence at high  $Re$ . From the definition of  $Re$ , one can deduce that turbulence is likely to occur in large bearings due to high surface velocity and relatively large clearance. Moreover, it often occurs when the bearing is lubricated by low viscosity process fluid, such as water. A turbulent bearing exhibits increased power consumption along with a sharp change of bearing eccentricity (Wilcock, 1950).

Compared to laminar flow, turbulent flow has increased stress due to the fluctuating motion. Since stress is proportional to viscosity, turbulent flow can be treated as laminar flow with increased effective viscosity, which is defined as the superposition of turbulent (eddy) viscosity and the actual viscosity of the lubricant. Thus, the Reynolds equation can be extended into the turbulent regime using effective viscosity values. Several models have been developed to evaluate the eddy viscosity. The models in Constantinescu (1959), Ng and Pan (1965), Elrod and Ng (1967), Safar and Szeri (1974) are similar in that they all utilize the “law of wall” in which the eddy viscosity is assumed as a function of wall shear stress and distance away from the wall. On the wall surface, the flow is laminar and there is no eddy viscosity contribution. The eddy viscosity increases as the position moves from the wall to the

core of the film. The specific formula used to quantify the eddy viscosity is different in those references. A distinct alternative is the bulk flow theory developed by Hirs (1973). Ignoring the detailed turbulence structure, his theory directly correlates the wall shear stress with the mean flow parameters using an empirical drag law. In addition, the fluctuating motion also enhances the heat transfer across the film. Analogous to the effective viscosity, an effective heat conductivity can be defined and employed to generalize the energy equation into turbulent flow regime.

Figure 35 shows maximum temperature and power loss as functions of shaft rotational speed. The experimental data represented by the discrete symbols are taken from Taniguchi et al. (1990). As shown in this figure, the  $T_{max}$  curve has a shift that corresponds to the flow regime transition: when the flow is laminar,  $T_{max}$  increases smoothly with the increasing shaft speed;  $T_{max}$  stays flat or even shows slight decrease during the flow regime transition;  $T_{max}$  resumes smooth increase after the transition is completed. Due to the increased effective heat conductivity, the analysis including turbulent effects yields lower and more accurate  $T_{max}$  predictions. The inclusion of turbulence also significantly improves the friction loss prediction. Bouard et al. (1996) compared three popular turbulent models: the Ng and Pan model, the Elrod and Ng model, and the Constantinescu model. They concluded that, if a bearing is turbulent, the turbulent effects must be taken into account and these three models gave similar results.

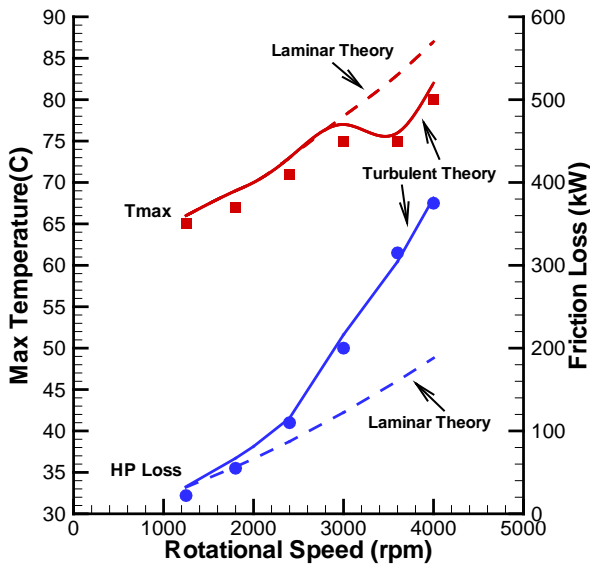


Figure 35. Comparisons of the Results from Turbulent and Laminar Theories (Experimental Results from Taniguchi et al, 1990)

#### Dynamic Coefficients

Section summary:

- The reduced coefficients of a tilting pad bearing are dependent on the shaft's precession or whirl frequency.

The bearing dynamic coefficients can be calculated by numerically perturbing the journal position or by solving the perturbed Reynolds equations. The first approach is straightforward. After establishing the steady state journal position, the hydrodynamic force is calculated at a slightly different position. Since the force is somewhat different at this new journal position, the force variation due to the small displacement is obtained and a stiffness coefficient is easily calculated from the definition of  $-\Delta F/\Delta x$ . A damping coefficient is similarly calculated with a velocity perturbation (apply a small  $\partial h/\partial t$  in Equation (12)). The second approach involves more mathematics because the perturbed Reynolds equations must be theoretically derived. Then, the dynamic coefficients are obtained by directly integrating the pressure solutions from those perturbed equations.

A fixed geometry bearing has eight dynamic coefficients because such journal-bearing system has only two degrees of freedom (the journal translation in X and Y). However, the dynamic system of a tilting pad bearing has more degrees of freedom because the pads can rotate. These extra degrees of freedom lead to additional dynamic coefficients that are related to the pads' tilting motion. For example, a five-pad tilting pad bearing has 58 dynamic coefficients. In practice, it is convenient to reduce these coefficients to eight equivalent ones that are related to journal's X and Y motions (Equation 7). This procedure is called dynamic reduction or dynamic condensation. As shown in Figure 36, the reduced coefficients are not constants, but dependent on the frequency of the shaft whirl, which means the shaft perceives different bearing stiffness and damping at each vibration frequency. A widely debated topic, more discussions on this frequency dependency can be found in Lund (1964), Parsell et al. (1983), API 684 (2005) and Cloud et al. (2012).

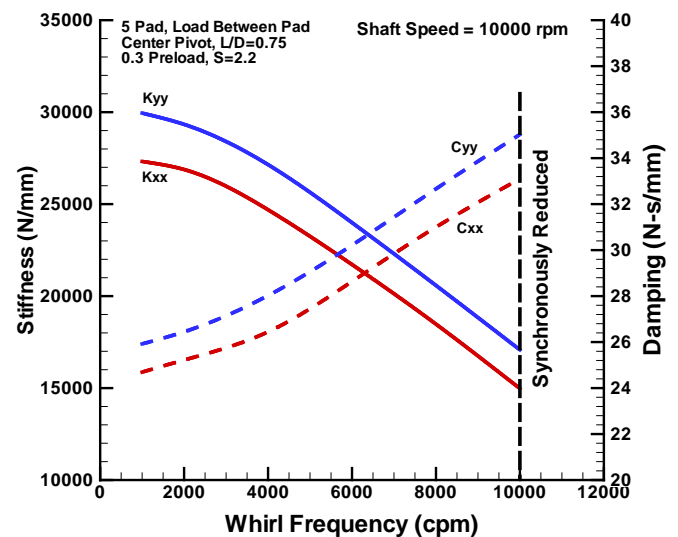
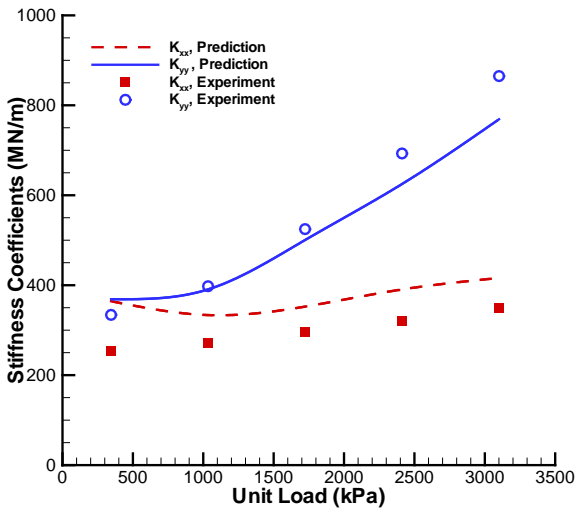


Figure 36. Frequency Dependent Stiffness and Damping Coefficients, Tilting Pad Bearing (Theoretical Prediction)

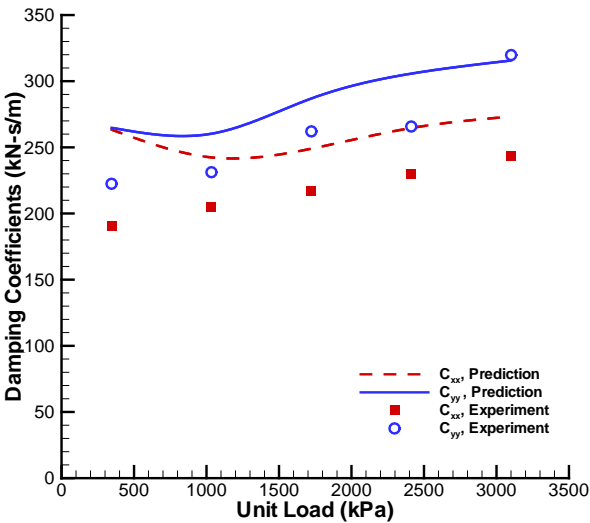


In Figure 37, the theoretically predicted coefficients are compared with experimental data for a tilting pad bearing. This bearing has 5 tilting pads with 60 percent pivot offset (Carter, 2007). The results presented here are obtained at 10,000 rpm shaft speed, with varying unit load from 50 psi (345 kPa) to 450 psi (3101 kPa) and load on pad orientation. The theoretical values were calculated by solving the perturbed Reynolds equations, and then, dynamically reduced at the synchronous frequency.

Depending on the computer program and how it is used, the predicted dynamic coefficients could show a wide range of scattering (Kocur, 2007). Therefore, it is important to validate and calibrate the analytical tool using available test data. More dynamic test data can be found in Dmochowski and Brockwell (1995), Harris (2008) and Kulhanek (2010).



(a)



(b)

Figure 37. Comparisons of Predicted and Measured Tilting Pad Bearing Dynamic Coefficients (Experimental Results from Carter, 2007)

### The Coupled Algorithm

Figure 38 shows the structure of a comprehensive, steady state thermoelastohydrodynamic (TEHD) algorithm that assembles the various models discussed above. The basic block is the classic hydrodynamic (HD) analysis. Since the film thickness  $h$  is required in the Reynolds equation, the journal operating position must be known in order to calculate the hydrodynamic pressure. However, we only know that the journal is operating at equilibrium where the resulting hydrodynamic force balances the external load. Therefore, the Reynolds equation is initially solved with assumed journal position and the actual position is searched through iterations. If a pad can tilt, its tilt angle also needs to be iteratively determined using the fact that, at equilibrium, the moment about the pivot must be zero.

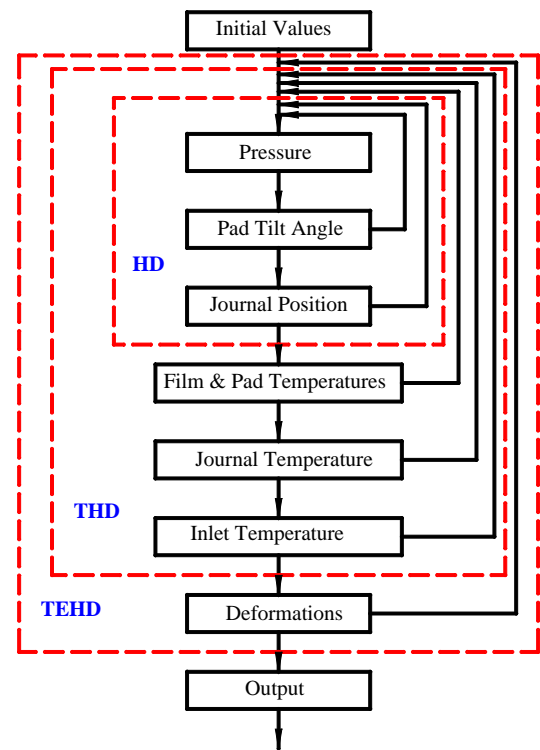


Figure 38. Structure of a Sample TEHD Algorithm

From the HD block, the algorithm can be expanded to a higher level that includes the thermal effects on the lubricant viscosity. As mentioned earlier, the energy equation must be added to the formulation and iteratively solved with the HD block. In addition, the journal and pad inlet temperatures also need to be calculated as important boundary conditions. During a revolution, a point on the journal surface travels across the hot and cool sections of the fluid film. Thus, it is reasonable to assume that the journal acquires the average film temperature and is constant. According to this model, heat flows into the journal in the hot sections, dumped back into the fluid film in the cool sections, and the journal is adiabatic in a bulk sense.

The pad inlet temperature is determined in the preceding oil groove (Heshmat and Pinkus, 1986). As shown in Figure 39, two

streams of lubricant are mixed in the groove: cool lubricant from the supply line and hot lubricant carried over from the previous pad. Therefore, at the pad inlet, the lubricant temperature is at some mixing value, which can be calculated by applying energy conservation to the groove control volume. Including various deformation models, the THD block can be further extended to a complex thermoelastohydrodynamic (TEHD) analysis. It should be pointed out that the structure shown in Figure 38 is not unique. People have used a variety of structures to achieve the same objective. However, regardless of the specific structure, a computation always begins with a group of assumed initial values, and ends after convergence has been reached for every iteration loop.

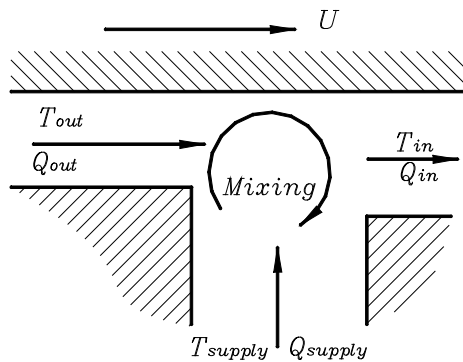


Figure 39. Mixing in an Oil Groove

### Special Situations

In some special applications, the TEHD models presented above are not sufficient to predict a bearing's properties. Direct lubrication and starvation require additional modeling efforts in order to achieve satisfactory theoretical predictions.

#### Direct Lubrication

Excessively high pad temperature is a problem in rotating machinery operations. One solution to this problem is the use of direct lubrication designs, such as those with an inlet pocket or spray bar. As suggested by the name, the idea is to directly supply cool oil into the pad clearance and block hot oil carry over from the previous pad. According to Figure 39, more  $Q_{supply}$  and less  $Q_{out}$  will lead to lower mixing temperature  $T_{in}$ , and consequently, lower temperature on the ensuing pad. Such direct lubrication designs have been successfully used and are gaining popularity in industry (Edney et al., 1998; DeCamillo and Brockwell, 2001).

Following this idea, Brockwell et al. (1994) developed a new groove mixing model for pad with an inlet pocket assuming all cool oil in the inlet pocket enters the film. Since such model yields significantly reduced inlet temperature, lower pad temperature is predicted in their THD analysis. Their predicted peak temperatures also had good agreement with their experimental data.

Later, He et al (2002) noticed several interesting trends in the same group of inlet pocket test data. First, compared to a conventional pad, an inlet pocket pad does not always have lower

temperature near its leading edge; instead, it consistently shows a smaller temperature gradient in the circumferential direction, which leads to the reduced peak temperature. This trend is clearly displayed in Figure 40. Second, on the curves of maximum temperature versus shaft speed, some flat sections are observed, and before those flat sections, the pocketed and conventional pads often have similar peak temperatures. As shown in Figure 35, the flat sections are likely the indicator of flow regime transition.

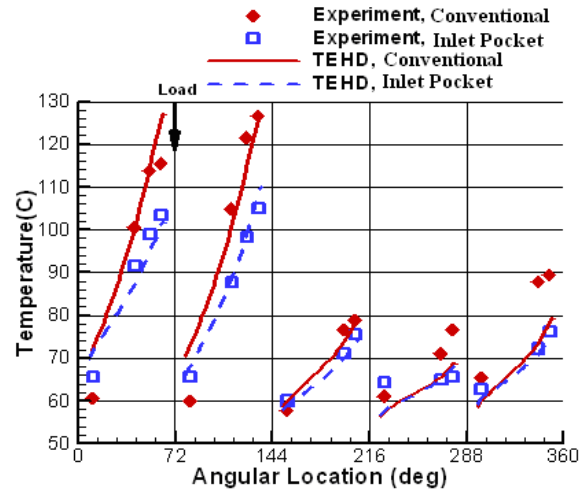


Figure 40. Pad Temperature Comparisons between Conventional and Inlet Pocket Bearings (Experimental Results from Brockwell et al.,1994)

To simulate these experimental trends for bearings with inlet pockets, He et al. (2002) proposed a different theory that attributes the cooling effects to turbulent flow that elevates heat transfer. According to their model, the inlet pocket destabilizes the flow and causes early turbulence onset. Figure 40 shows the theoretical results that employed their triggered turbulence model, where the predicted pad temperatures have close agreement with Brockwell's experimental data. However, He et al. (2002) did not identify the trigger that prompts turbulence on an inlet pocket pad.

Even though direct lubrication designs have become very popular, their cooling mechanisms are still not clear and subject to debate (Grzegorz and Michal, 2007; He et al., 2012). More work needs to be done to understand their underlying physics and improve their theoretical modeling.

#### Starvation

With an evacuated housing, lubricant needs to be continuously supplied into a bearing to replenish the side leakage. With enough oil, a continuous fluid film is always established at the leading edge of a pad that has convergent clearance. This situation is schematically shown in Figure 41 (a).

However, an evacuated bearing can also be working in a starved condition in which the amount of oil is not enough to fill the pad leading edge clearance, meaning the inlet region is

cavitated. As shown in Figure 41 (b), it is reasonable to assume that the continuous film is formed a certain distance away from the inlet where the clearance is sufficiently reduced. Figure 41 also shows conventional cavitation that is caused by divergent clearance near the pad trailing edge. Examples of starved applications include ring-lubricated bearings and direct lubrication designs which may be starved to minimize power consumption (Heshma and Pinkus, 1985; Brockwell et al., 1994).

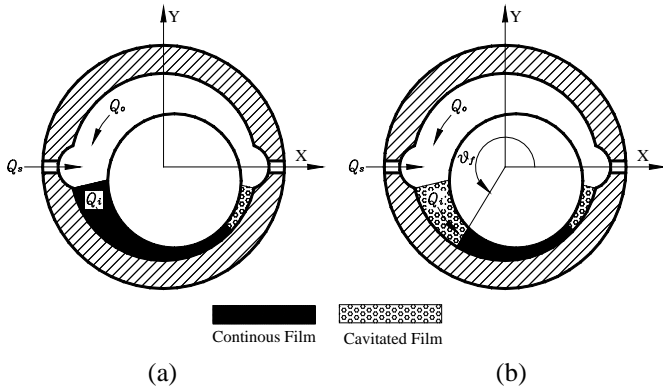


Figure 41. Flooded and Starved Lubrication Conditions

Based on Figure 41 (b), one method to model starvation is to determine the continuous film onset angle  $\theta_f$ . If  $\theta_f$  is known, the bearing can be analyzed using the standard models and the effective arc length from  $\theta_f$  to the trailing edge.  $\theta_f$  can be iteratively determined by comparing the available and required flow rates: at a certain location, if more lubricant is available to fill the clearance, the predicted  $\theta_f$  should be upstream where the larger clearance can accommodate the extra fluid; otherwise, the available lubricant can only fill a smaller space and  $\theta_f$  should be predicted further downstream (He et al., 2005). Clearly, this search is coupled with the search of journal position.

For a multi-pad bearing, the level of starvation is different on each pad because a loaded pad has smaller operating clearance compared to an unloaded one. Therefore, starvation tends to occur on the unloaded pads first, and gradually spread onto the loaded pads. It also means that required pad flow is a function of eccentricity (or load) and speed, and different for each pad. Since pad flow is usually controlled by inlet orifices preceding each pad, the flow to each pad can be tailored, but only for a single load/speed condition. Also, note that the unloaded pads require more oil flow than the loaded pads.

As shown in Figure 42, when the bearing has 100 percent supply flow, hydrodynamic pressure is developed on all pads because the unloaded top pads have 0.6 offset pivots. The hydrodynamic forces on those pads are labeled as  $F_1$  to  $F_5$ , respectively. When the total supply flow rate to the entire bearing is cut by half, pad #3 and #4 are totally starved and pad #5 exhibits a 6.7 percent starvation region, the two bottom pads are still flooded. When the flow rate is reduced to 40 percent, the starvation region on pad #5 is expanded to 10 percent and pad #2 has a 6.7 percent starvation region. If the flow rate is further

reduced to 30 percent, pad #5 becomes 100 percent starved and a 13.3 percent starvation area shows up on pad #2.

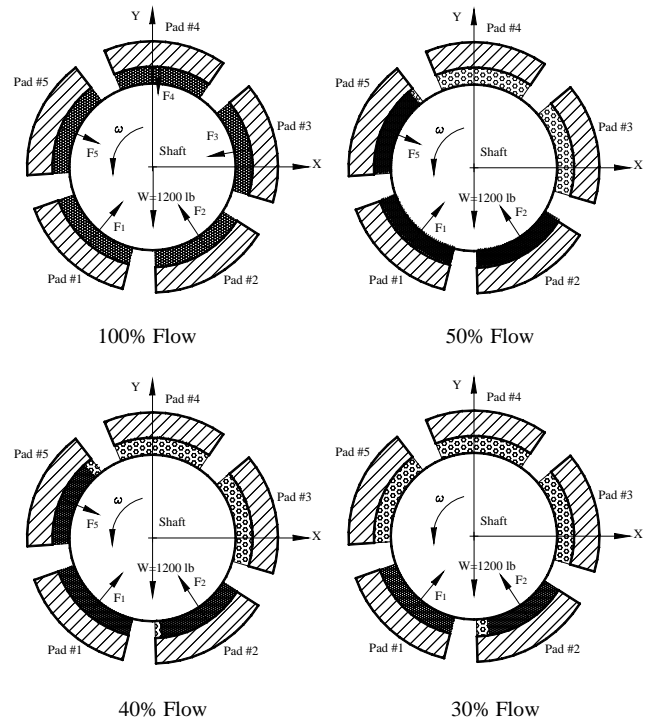


Figure 42. Progression of Starvation in a Five-Pad Tilting Pad Bearing (Courtesy He et al., 2005)

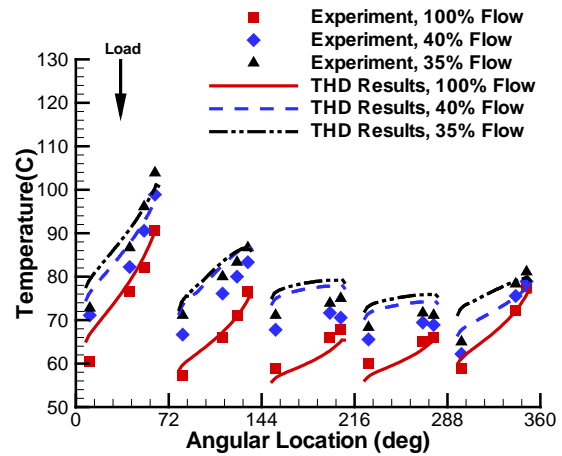


Figure 43. Pad Temperature versus Flowrate (Experimental Results from Brockwell et al., 1994)

A starved bearing exhibits increased temperature and decreased friction loss. As shown in Figures 43 and 44, the pad temperature is increasing as the bearing becomes more and more starved. However, since starvation leads to reduced continuous film area, the power loss due to viscous shearing is decreased. Besides higher temperature, starvation also reduces a bearing's load capacity and stiffness. An example in He et al. (2005) shows

that a bearing's horizontal stiffness  $K_{xx}$  can quickly diminish as the result of overly reduced flow rate. In addition, starvation may result in dry friction rubs (which may excite shaft vibration), pad flutter (which may damage the fluttering pads), or subsynchronous vibration hash (DeCamillo et al, 2008).

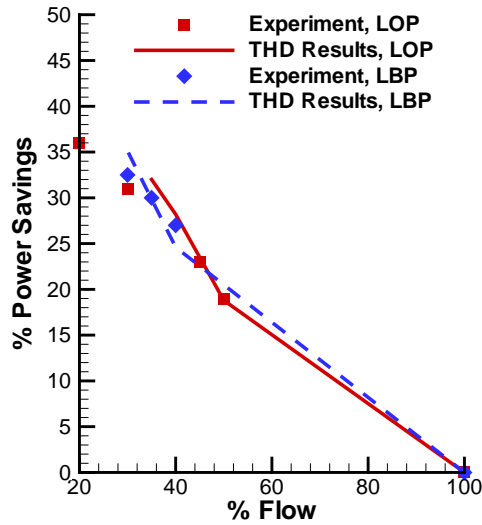


Figure 44. Power Savings versus Flowrate (Experimental Results from Brockwell et al., 1994)

#### Additional Comments on Modeling

Modern TEHD theories generally can give satisfactory predictions for a bearing's performance parameters. A variety of computer programs have been developed and successfully used in bearing design and analysis. Although significant progress has been made since Osborne Reynolds, bearing modeling still faces a number of challenges. To name a few:

- Temperature boundary conditions. In thermal analysis, the difficult task is not to write down the equations, but to assign appropriate boundary conditions. The most important one is the film inlet temperature that is governed by groove mixing shown in Figure 39. A detailed modeling of the three-dimensional flow is impractical, and would involve turbulence, heat exchange with the solids, and possible two-phase flow of liquid and air. Therefore, as mentioned earlier, a simple equation based on energy balance is used as a practical approximation. In this model, a hot oil carryover factor is required to address the fact that not all exit flow  $Q_{out}$  enters the next pad. The hot oil carryover factor, which is a function of the bearing design and operation condition, cannot be accurately obtained. Instead, it is usually estimated between 75-100 percent based on experience. Therefore, significant error can be introduced as the result of a poor estimate. Errors are also introduced on the back of a pad where heat convection boundary condition is usually applied. Similar to the hot oil carryover factor, the convection coefficient is unknown and often specified from an engineers' best estimate. In some situations, such as misaligned shaft and bearing, the axial temperature cannot be assumed constant. The full three-

dimensional energy equation must be employed, which leads to the difficulty of determining the boundary conditions at the axial ends.

- Deformation boundary conditions. As discussed above, to accurately model the journal and outer shell deformations, the shaft and bearing housing need to be taken into account. However, the shaft and housing conditions are difficult to obtain and they are dependent on a machine's specific design and operation. Their modeling essentially goes beyond the scope of a bearing analysis.
- Flow regime transition. To analyze a possibly turbulent bearing, the difficult question is when to apply the turbulence model. In most analyses, two critical Reynolds numbers are employed to determine flow regime transition. If the actual  $Re$  in the bearing is smaller than the lower critical Reynolds number, the flow is considered laminar; if  $Re$  is larger than the upper critical Reynolds number, the flow is modeled as full turbulence; if  $Re$  is between those two threshold numbers, the flow is transitional and the eddy viscosity is scaled by a percentage factor (Suganami and Szeri, 1979). However, there is no reliable way to determine those critical  $Re$ 's. Although they are usually prescribed as constants, studies have indicated that they are functions of bearing geometry and operating condition (Xu, 1993). Again, large errors can be introduced if a modeling is based on an incorrect flow regime assumption.
- Complex geometries. These include the inlet pockets, spray bars, by-pass cooling grooves and hydrostatic lift pockets for startup. Future research is needed to investigate these more complex designs.

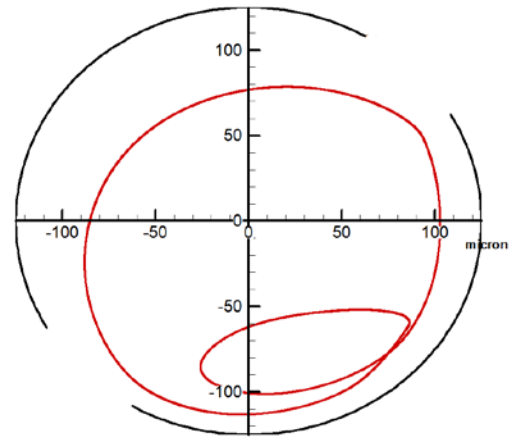


Figure 45. Non-linear, Time Transient Simulation of Large Shaft Motion to Determine Babbitt Life

- Non-linear, time transient analysis. This tutorial focuses on the operation and modeling of a bearing experiencing relatively small vibrations as a percentage of its clearance, represented by the situation depicted in Figure 20. However, if the shaft experiences large vibrations like that shown in Figure 21, non-linear, time transient analysis must be performed to predict the bearing's performance. Figure 45 shows an example of such an analysis. In this case, the large



multi-frequency orbit was simulated to assess the fatigue risk of bearing Babbitt. Such simple transient analysis has been conducted for many years. However, most of them were limited to isoviscous and fixed geometry bearings. Full analysis with thermal and elastic effects on tilting pad bearings has not become mainstream due to the substantially higher computational cost. Discussions on transient analysis can be found in Paranjpe and Han (1995).

## CONCLUSIONS

In this tutorial, major areas of journal bearings' operation and modeling are discussed. With respect to the operational aspects, we have learned that

- A bearing's load carrying capacity comes from the hydrodynamic pressure developed in the fluid film.
- A convergent wedge, a moving surface and a viscous lubricant are necessary to generate hydrodynamic force in steady state operation.
- Hydrodynamic forces have cross-coupled components which lead to large attitude angle and stability issues for fixed geometry bearings.
- Due to the pads' ability to tilt, tilting pad bearings have minimum cross-coupled forces and stiffnesses, which leads to their superior dynamic performance.
- Viscous shearing generates heat in the film, which leads to temperature rise and viscosity reduction.
- Hydrodynamic pressure and temperature rise cause elastic deformations that change the film shape.
- Viscous shearing also results in mechanical power loss.
- Many bearings work in a flooded lubrication condition. However, a bearing may be operating in a starved condition if it has an evacuated housing and insufficient oil supply flowrate. Starvation is not necessarily unacceptable. However, the bearing's performance needs to be carefully evaluated.
- For relatively small vibrations like those normally encountered, a bearing's dynamic properties can be represented by linear springs and dampers.
- Direct stiffness, direct damping and cross-coupled stiffness coefficients have significant rotordynamic implications.
- Dynamically, it is important to remember that a bearing is part of a *global* system involving rotor, seals, supports, etc.
- There are two predominant categories of vibration instability: oil whirl and shaft whip. Associated only with fixed geometry bearings, the former is largely determined by the bearing properties and load. Applicable to either type of bearing, shaft whip is governed by the combined system.
- Both steady state and dynamic characteristics are speed and load dependent.

To predict a bearing's performance, theoretical models have been developed and successfully used in industry. The major models and mainstream techniques can be summarized as following:

- A theoretical model that includes pressure, temperature and elasticity effects is often called thermoelastohydrodynamic

(TEHD) algorithm. When properly used, a TEHD analysis can yield good prediction of a bearing's performance.

- Pressure calculations are the foundation of a TEHD algorithm. The Reynolds equation is usually employed in computer programs.
- For most analysis, thermal effects must be taken into account. A computer code usually solves some form of the energy equation.
- The elastic deformations should be included in the analysis of high speed, heavily loaded bearings. However, the models need to be used with caution.
- A turbulence model must be available to accurately predict the properties of a turbulent bearing. Turbulent flow is usually associated with large bearing size, high shaft speed and low lubricant viscosity.
- For tilting pad bearings, the dynamic coefficients can be highly frequency dependent.
- Most TEHD algorithms cannot be applied to predict direct lubricated or starved bearings. These special cases require additional modeling enhancements.
- Current state-of-the-art bearing modeling still faces a variety of difficulties and challenges.

## NOMENCLATURE

- $c$  = Bearing clearance
- $c_b$  = Assembled clearance
- $c_p$  = Pad machined clearance
- $c_o$  = Nominal bearing clearance
- $\Delta c$  = Clearance variation due to deformation
- $C_{ij}$  = Damping coefficients,  $i, j = X$  or  $Y$
- $C_p$  = Lubricant specific heat
- $D$  = Journal diameter
- $e$  = Journal eccentricity
- $e_X$  = Journal eccentricity projected on horizontal (X) axis
- $e_Y$  = Journal eccentricity projected on vertical (Y) axis
- $E$  = Journal eccentricity ratio
- $E_X$  = Journal eccentricity ratio projected on horizontal (X) axis
- $E_Y$  = Journal eccentricity ratio projected on vertical (Y) axis
- $F_x$  = Film force in horizontal (X) direction
- $F_y$  = Film force in vertical (Y) direction
- $h$  = Film thickness
- $h_i$  = Film thickness at wedge inlet
- $h_o$  = Film thickness at wedge outlet
- $K_{ij}$  = Stiffness coefficients,  $i, j = X$  or  $Y$
- $L$  = Bearing axial length
- $m$  = Pad preload
- $O_b$  = Bearing center
- $O_p$  = Pad arc center
- $O_J$  = Journal center
- $p$  = Pressure
- $Q$  = Flowrate
- $R$  = Journal radius
- $R_b$  = Bearing set bore radius
- $R_p$  = Pad set bore radius



$R_j$  = Journal radius  
 $Re$  = Reynolds number  
 $S$  = Sommerfeld Number  
 $T$  = Temperature  
 $T_{max}$  = Maximum pad temperature  
 $T$  = Time  
 $U$  = Journal surface velocity  
 $u$  = Fluid velocity in circumferential (x) direction  
 $v$  = Fluid velocity in radial (y) direction  
 $W$  = Applied load  
 $W_U$  = Unit load ( $W_U = W/(L \cdot D)$ )  
 $w$  = Fluid velocity in axial (z) direction  
 $X$  = Horizontal direction  
 $Y$  = Vertical direction  
 $x$  = Circumferential direction along a pad  
 $y$  = Radial direction across film  
 $z$  = Axial direction along a pad  
 $\alpha$  = Pad offset factor  
 $\beta$  = Angle measured from leading edge to the pivot location  
 $\Phi$  = Journal attitude angle  
 $\kappa$  = heat conductivity  
 $\mu$  = Lubricant viscosity  
 $\theta_p$  = Pad arc length  
 $\rho$  = Lubricant density  
 $\tau$  = Shear stress  
 $\omega$  = Shaft rotational speed

## REFERENCES

- API 684, 2005, "Tutorial on Rotordynamics: Lateral Critical, Unbalance Response, Stability, Train Torsional and Rotor Balancing," Second Edition, American Petroleum Institute, Washington, D.C.
- Barrett, L. E., Gunter, E. J., and Allaire, P. E., 1978, "Optimum Bearing and Support Damping for Unbalance Response and Stability of Rotating Machinery," *ASME Journal of Engineering for Power*, 100(1), pp. 89-94.
- Bouard, L., Fillon, M. and Frene, J., 1996, "Comparison between Three Turbulent Models – Application to Thermohydrodynamic Performances of Tilting-Pad Journal Bearings", *Tribology International*, 29, pp. 11-18.
- Boyd, J. and Raimondi, A. A., 1953, "An Analysis of the Pivoted-Pad Journal Bearing," *Mechanical Engineering*, 75, pp. 380-386.
- Brechtling, R., 2002, "Static and Dynamic Testing of Tilting Pad Journal Bearings as a Function of Load Angle and Journal Speed", Master Thesis, University of Virginia.
- Brockwell, K., Dmochowski, W., and Decamillo, S., 1994, "Analysis and Testing of the LEG Tilting Pad Journal Bearing- a New Design for Increasing Load Capacity, Reducing Operating Temperatures and Conserving Energy", *Proc. of the 23<sup>rd</sup> Turbomachinery Symposium*, Turbomachinery Laboratory, Texas A&M University, College Station, Texas, pp. 43-56.
- Brugier, D. and Pascal, M., 1989, "Influence of Elastic Deformations of Turbo-Generator Tilting Pad Bearing on the Static Behavior and on the Dynamic Coefficients in Different Designs", *Journal of Tribology*, 111, pp. 364-371.
- Byrne, J. M. and Allaire, P. E., 1999, "Optimal Design of Fixed Pad Fluid Film Bearings for Load Capacity, Power Loss, and Rigid Rotor Stability," Report No.UVA/643092/MAE98/530, ROMAC Laboratories, University of Virginia.
- Carter, C., R., 2007, "Measured and Predicted Rotordynamic Coefficients and Static Performance of a Rocker-Pivot, Tilt Pad Bearing in Load-on-Pad and Load-between-Pad Configurations", Master's Thesis, Texas A & M University.
- Cloud, C., Maslen, E. and Barrett, L., 2012, "Rotor Stability Estimation with Competing Tilting Pad Bearing Models", *Mechanical Systems and Signal Processing*, 29, pp. 90-106.
- Constantinescu, V., 1959, "On Turbulent Lubrication", *Proceedings of the Institution of Mechanical Engineers*, 173, pp. 881-900.
- Cope, W., 1949, "The Hydrodynamic Theory of Film Lubrication", *Proc. Royal Soc. (London) Ser. A*, 197, pp. 201-217.
- DeCamillo, S. and Brockwell, K., 2001, "A Study of Parameters That Affect Pivoted Shoe Journal Bearing Performance in High-Speed Turbomachinery," *Proceedings of the 30<sup>th</sup> Turbomachinery Symposium*, Turbomachinery Laboratory, Texas A&M University, College Station, Texas, pp. 9-22
- DeCamillo, S., He, M., Cloud, C. and Byrne, J, 2008, "Journal Bearing Vibration and SSV Hash," *Proceedings of the 37<sup>th</sup> Turbomachinery Symposium*, Turbomachinery Laboratory, Texas A&M University, College Station, Texas, pp. 11-23
- Desbordes, H., Fillon, M. Wai, C. and Frene, J., 1994, "Dynamic Analysis of Tilting-Pad Journal Bearing - Influence of Pad Deformations", *Journal of Tribology*, 116, pp. 621-628.
- Dmochowski, W. and Brockwell, K., 1995, "Dynamic Testing of the Tilting Pad Journal Bearing", *Tribology Transactions*, 38, pp. 261-268
- Dowson, D., 1962, "A Generalized Reynolds Equation for Fluid Film Lubrication", *International Journal of Mechanical Science*, 4, pp. 159-170.



- Dowson, D., 1998, *History of Tribology*, 2<sup>nd</sup> Edition, Profession Engineering Publishing Ltd., Suffolk, UK.
- Dowson, D. and Hudson, J., 1963, "Thermo-Hydrodynamic Analysis of the Infinite Slider Bearing: Part II – The Parallel Surface Bearing", *Lubrication and Wear Convention, Institution of Mechanical Engineering*, Paper 4 and 5.
- Edney, S., Heitland, G.B., and Decamillo, S., 1998, "Testing, Analysis, and CFD Modeling of a Profiled Leading Edge Groove Tilting Pad Journal Bearing", *Presented at the International Gas Turbine & Aeroengine Congress & Exhibition*, Stockholm, Sweden, June 2-5.
- Ehrich, F. F., and Childs, D. W., 1984, "Self-Excited Vibration in High-Performance Turbomachinery," *Mechanical Engineering*, May, pp. 66-79.
- Elrod, H. and Ng, C., 1967, "A Theory for Turbulent Fluid Films and Its Application to Bearings", *Journal of Lubrication Technology*, 89, pp. 346-362.
- Elwell, R.C. and Booser, E.R., 1972, "Low-Speed Limit of Lubrication – Part One: What is a 'Too Slow' Bearing?," *Machine Design*, June 15, pp. 129-133.
- Ettles, C., 1980, "The Analysis and Performance of Pivoted Pad Journal Bearings Considering Thermal and Elastic Effects", *Journal of Lubrication Technology*, 102, pp. 182-192.
- Fillon, M., Bligoud, J. and Frene, J., 1992, "Experimental Study of Tilting-Pad Journal Bearings - Comparison with Theoretical Thermoelastohydrodynamic Results", *Journal of Tribology*, 114, pp. 579-587.
- Fitzgerald, M. and Neal, P., 1992, "Temperature Distributions and Heat Transfer in Journal Bearings", *Journal of Tribology*, 114, pp. 122-130.
- Gardner, W.W., 1976, "Journal Bearing Operation at Low Sommerfeld Numbers," *ASLE Transactions*, 19, No.3, pp. 187-194.
- Grzegorz, R. and Michal, W., 2007, "CFD Analysis of the Lubricant Flow in the Supply Groove of a Hydrodynamic Thrust Bearing Pad," *Proceedings of ASME/STLE International Joint Tribology Conference*, San Diego, California USA, October 22-24.
- Hagg, A. C., 1946, "The Influence of Oil-Film Journal Bearings on the Stability of Rotating Machinery," *ASME Transactions, Journal of Applied Mechanics*, 68, pp. A211-A220.
- Hamrock, B. J., 1994, *Fundamentals of Fluid Film Lubrication*, McGraw-Hill.
- Harris, J., M., 2008, "Static Characteristics and Rotordynamic Coefficients of a Four-Pad Tilting-Pad Journal Bearing with Ball-in-Socket Pivots in Load-between-Pad Configuration", *Master's Thesis*, Texas A & M University.
- He, M., Allaire, P., Barrett, L. and Nicholas, J., 2002, "TEHD Modeling of Leading Edge Groove Journal Bearings", *IFTOMM, Proc. of 6<sup>th</sup> International Conference on Rotor Dynamics*, 2, pp. 674-681.
- He, M., Allaire, P., Cloud, C. H., and Nicholas, J., 2004, "A Pressure Dam Bearing Analysis with Adiabatic Thermal Effects", *Tribology Transactions*, 47, pp. 70-76.
- He, M., Allaire, P., Barrett, L. and Nicholas, J., 2005, "THD Modeling of Leading Edge Groove Bearings under Starvation Condition", *Tribology Transactions*, 48, pp. 362-369.
- He, M., Byrne, J, Cloud, C. and Vazquez, J., 2012, "Steady State Performance Predictions of Directly Lubricated Fluid Film Journal Bearings", *Proceedings of the 41<sup>st</sup> Turbomachinery Symposium*, Turbomachinery Laboratory, Texas A&M University, College Station, Texas
- Heshmat, H., 1991, "The Mechanism of Cavitation in Hydrodynamic Lubrication", *Tribology Transactions*, 34, pp. 177-186.
- Heshmat, H., and Pinkus, O., 1985, "Performance of Starved Journal Bearings with Oil Ring Lubrication", *Journal of Tribology*, 107, pp. 23-32.
- Heshmat, H. and Pinkus, O., 1986, "Mixing Inlet Temperatures in Hydrodynamic Bearings", *Journal of Tribology*, 108, pp. 231-248.
- Hirs, G., 1973, "A Bulk-Flow Theory for Turbulence in Lubricant Film", *Journal of Lubrication Technology*, 95, pp. 137-146.
- Hummel, C., 1926, "Kristische Drehzahlen als Folge der Nachgiebigkeit des Schmiermittels im Lager," *VDI-Forschungsheft* 287.
- Jones, G. J. and Martin, F. A., 1979, "Geometry Effects in Tilting-Pad Journal Bearings," *STLE Tribology Transactions*, 22, pp. 227-244.
- Kim, J., Palazzolo, A. and Gadangi, R., 1994, "TEHD Analysis for Tilting-Pad Journal Bearings Using Upwind Finite Element Method", *Tribology Transactions*, 37, pp. 771-783.



- Kirk, R., and Reedy, S., 1988, "Evaluation of Pivot Stiffness for Typical Tilting-Pad Journal Bearing Design", *Journal of Vibration, Acoustics, Stress, and Reliability in Design*, 110, pp. 165-171.
- Kocur, J., Nicholas, J. and Lee, C., 2007, "Surveying Tilting Pad Journal Bearing and Gas Labyrinth Seal Coefficients and Their Effect on Rotor Stability," *Proceedings of the 26<sup>th</sup> Turbomachinery Symposium*, Turbomachinery Laboratory, Texas A&M University, College Station, Texas, pp. 1-10.
- Kulhanek, C., D., 2010, "Dynamic and Static Characteristics of a Rocker-Pivot, Tilting-Pad Bearing with 50% and 60% Offsets", Master's Thesis, Texas A & M University.
- Lanes, R. F., Flack, R. D., and Lewis, D. W., 1981, "Experiments on the Stability and Response of a Flexible Rotor in Three Types of Journal Bearings", *ASLE Transactions*, 25, No. 3, pp. 289-298.
- Lund, J., 1964, "Spring and Damping Coefficients for the Tilting Pad Journal Bearing", *ASLE Trans.*, 7, pp. 342-352.
- Lund, J. W., 1987, "Review of the Concept of Dynamic Coefficients for Fluid Film Journal Bearings," *ASME Journal of Tribology*, 109, pp. 37-41.
- Lund, J. and Pedersen, L., 1987, "The Influence of Pad Flexibility on the Dynamic Coefficients of a Tilting-Pad Journal Bearing", *Journal of Tribology*, 109, pp. 65-70.
- Lund J. and Saibel, E., 1967, "Oil Whip Whirl Orbits of a Rotor in Sleeve Bearings", *Journal of Engineering for Industry*, 89, pp 813-823.
- Martin, F. and Garner, G., 1973, "Plain Journal Bearings Under Steady Loads, Design Guidance for Safe Operation", *First European Tribology Congress*, pp. 1-16.
- McCallion, H., Yousif, F. and Lloyd, T., 1970, "The Analysis of Thermal Effects in a Full Journal Bearing", *Journal of Lubrication Technology*, 92, pp. 578-587.
- Muszynska, A., and Bently, D. E., 1995, "Fluid-Induced Instability of Rotors: Whirl and Whip – Summary of Results," Noise and Vibration Conference, Pretoria, South Africa.
- Newkirk, B. L., 1924, "Shaft Whipping," *General Electric Review*, 27(3), pp. 169-178.
- Newkirk, B. L., and Taylor, H. D., 1925, "Shaft Whipping due to Oil Action in Journal Bearings," *General Electric Review*, 28(8), pp. 559-568.
- Ng, C. and Pan, C., 1965, "A Linearized Turbulent Lubrication Theory", *Journal of Basic Engineering Ser. D*, 87, pp. 675-688.
- Nicholas, J., C., 1994, "Tilting-Pad Bearing Design", *Proceedings of the 23<sup>rd</sup> Turbomachinery Symposium*, Turbomachinery Laboratory, Texas A&M University, College Station, Texas, pp. 179-194.
- Nicholas, J. C., Gunter, E. J., and Barrett, L. E., 1978, "The Influence of Tilting Pad Bearing Characteristics on the Stability of High-Speed Rotor Bearing Systems," Report No.UVA/643092/MAE81/141, ROMAC Laboratories, University of Virginia.
- Nicholas, J. and Wygant, K., 1995, "Tilting Pad Journal Bearing Pivot Design for High Load Application", *Proceeding of the 24<sup>th</sup> Turbomachinery Symposium*, Turbomachinery Laboratory, Texas A&M University, College Station, Texas, pp. 1-15.
- Paranjpe, R. S., and Han, T., 1994, "A Study of the Thermohydrodynamic Performance of Steadily Loaded Journal Bearings", *Tribology Transactions*, 37, pp. 679-690.
- Paranjpe, R. S., and Han, T., 1995, "A Transient Thermohydrodynamic Analysis Including Mass Conserving Cavitation for dynamically Loaded Journal Bearings", *Journal of Tribology*, 117, pp. 369-378.
- Parsell, J. K., Allaire, P. E., and Barrett, L. E., 1983, "Frequency Effects in Tilting-Pad Journal Bearing Dynamic Coefficients", *ASLE Transactions*, 26, pp. 222-227.
- Petrov, N., 1883, "Friction in Machines and the Effect of the Lubricant", *Inzhenernii Zhurnal*, St. Petersburg, 1, pp. 71-104, 2, pp. 227-279, 3, pp. 377-436, 4, pp. 435-464 (In Russian).
- Pinkus, O., 1987, "The Reynolds Centennial: A Brief History of the Theory of Hydrodynamic Lubrication," *ASME Journal of Tribology*, 109, pp. 2-20.
- Raimondi, A. and Boyd, J., 1958, "A Solution of the Finite Journal Bearing and Its Application to Analysis and Design – Part III", *Trans. ASLE*, 1, pp. 159-209.
- Reynolds, O., 1886, "On the Theory of Lubrication and Its Applications to Mr. Beauchamp Tower's Experiments Including an Experimental Determination of the Viscosity of Olive Oil," *Philosophical Transactions*, 177, pp. 157-234.
- Safar, Z., and Szeri, A. Z., 1974, "Thermohydrodynamic Lubrication in Laminar and Turbulent Regimes", *Journal of Lubrication Technology*, 96, pp. 48-56.



- Salamone, D. J., 1984, "Journal Bearing Design Types and Their Applications to Turbomachinery," *Proceedings of the 13<sup>th</sup> Turbomachinery Symposium*, Turbomachinery Laboratory, Texas A&M University, College Station, Texas, pp. 179-188.
- Seireg, A. and Ezzat, H., 1973, "Thermohydrodynamic Phenomena in Fluid Film Lubrication", *Journal of Lubrication Technology*, 95, pp. 187-194.
- Simmons, J. and Lawrence, C., 1996, "Performance Experiments with 200 mm, Offset Pivot Journal Pad Bearing", *Tribology Transactions*, 39, pp. 969-973.
- Stodola, A., 1925, "Kristische Wellenstörung infolge der Nachgiebigkeit des Oelpolsters im Lager," *Schweizerische Bauzeitung*, 85, pp. 265-266.
- Suganami, T., and Szeri, A. Z., 1979, "A Thermohydrodynamic Analysis of Journal Bearings", *Journal of Lubrication Technology*, 101, pp. 21-27.
- Szeri, A., 1979, "Tribology – Friction, Lubrication, and Wear", McGraw-Hill Book Company.
- Taniguchi, S., Makino, T., Takeshita, K., and Ichimura, T., 1990, "A Thermohydrodynamic Analysis of Large Tilting-Pad Journal Bearing in Laminar and Turbulent Flow Regimes with Mixing", *Journal of Tribology*, 112, pp. 542-550.
- Tower, B., 1883, "First Report on Friction Experiments," *Proceedings Institute of Mechanical Engineering*, pp. 632-666.
- Tower, B., 1885, "Second Report on Friction Experiments," *Proceedings Institute of Mechanical Engineering*, pp. 58-70.
- Wilcock, D., 1950, "Turbulence in High Speed Journal Bearings", *Transactions of the ASME*, 72, pp. 825-834.
- Xu, H. and Zhu, J., 1993, "Research of Fluid Flow and Flow Transition Criteria from Laminar to Turbulent in a Journal Bearing", *Journal of Xi'An Jiaotong University*, 27, pp. 7-14.
- Zuck, C. and Flack, R., 1986, "Experiments on the Stability of an Overhung Rotor in Pressure-Dam and Multilobe Bearings", *ASLE Transactions*, 30, pp. 225-232.